
	<p>Research and Development Programme on Seismic Ground Motion</p> <p>CONFIDENTIAL <i>Restricted to SIGMA scientific partners and members of the consortium, please do not pass around</i></p>	<p>Ref : SIGMA-2013-D2-72 Version : 01</p> <p>Date : Page :</p>
--	---	---



CALIBRATION OF GMPEs FOR PO PLAIN REGION

AUTHORS			REVIEW			APPROVAL		
NOM	DATE	VISA	NOM	DATE	VISA	NOM	DATE	VISA
F. PACOR INGV Milano			A. Gurpinar	In written review attached		M. Corigliano		
			Ph. Renault (Swissnuclear)	In written review attached		G. Senfaute		

DISSEMINATION: Authors; Steering Committee; Work Package leaders, Scientific Committee, Archiving.


	Research and Development Programme on Seismic Ground Motion		Ref : SIGMA-2013-D2-72 Version : 01
	CONFIDENTIAL <i>Restricted to SIGMA scientific partners and members of the consortium, please do not pass around</i>		Date : 15 may Page : 1



CALIBRATION OF GMPEs FOR PO PLAIN REGION

AUTHORS			REVIEW			APPROVAL		
NOM	DATE	VISA	NOM	DATE	VISA	NOM	DATE	VISA
F. PACOR L. LUZI R. PUGLIA M. D'AMICO INGV Milano	15 May <i>F. Pacor</i>		A. Gurpinar			M. Corigliano		
			Ph. Renault	7.6.2013 <i>Ph. Renault</i>		G. Senfaute		

DISSEMINATION: Authors; Steering Committee; Work Package leaders, Scientific Committee, Archiving.

	<p style="text-align: center;">Research and Development Programme on Seismic Ground Motion</p> <p style="text-align: center;">CONFIDENTIAL <i>Restricted to SIGMA scientific partners and members of the consortium, please do not pass around</i></p>	<p>Ref : SIGMA-2013-D2-72 Version : 01</p> <p>Date : 15 may Page : 2</p>
--	--	--

Executive Summary

Every new earthquake reveals new features of the seismic ground motion, that were not taken into account in previous models because of paucity of instrumental observations. The 2012 Emilia seismic sequence occurred in the Po plain (northern Italy) provided a huge quantity of new strong-motion data. The analysis of these records allows us to acquire new insights on the ground motion in a poorly investigated area. The aim of this work is the compilation of a qualified strong-motion dataset for northern Italy and the calibration of regional ground motion prediction equations (GMPEs).

The dataset, called DBN2, is an updated version of DBN released in November 2012, and is composed by 2174 waveforms, recorded in the period 1976 (Friuli sequence) – 2012 (Emilia sequence). It includes 136 earthquakes (109 of them recorded by more than 1 stations) and 299 stations (248 of them having more than 1 records) in the magnitude range 3.5-6.4. The Emilia seismic sequence provides about the 2/3 of the entire dataset of northern Italy.

We present a set of equations derived for the geometrical mean of the horizontal components and the vertical component, considering the updated strong motion database for northern Italy, hereinafter DBN2.


The regressions are performed over the magnitude range 4–6.4 and considering both Joyner and Boore and hypocentral distances up to 200 km and depths up to 30km.

The equations are derived for peak ground acceleration (PGA) and 5%-damped spectral acceleration at periods between 0.04 and 4 s.

The total standard deviation (σ) varies between 0.32 and 0.41 log10 unit, The total standard deviation (σ_{tot}) varies between 0.32 and 0.41 log10 unit, with the largest values observed at short periods.


This set of new GMPEs improves the existing attenuation equation derived for northern Italy, however it should be used with some recommendations, since the compiled North Italy data set is characterized by an unbalanced number of recordings (majority of thrust or reverse style of faulting, class A and B sites at large distance and C1 sites at short distances).

As a consequence, the GMPEs derived in this study are proposed to evaluate the PGA and spectral ordinates in the Po plain area especially for C1 sites and thrust faults. For the rest of the cases (other styles of faulting and soil categories) the use of the GMPEs derived by Bindi et al (2011) for the Italian territory is recommended.

	<p style="text-align: center;">Research and Development Programme on Seismic Ground Motion</p> <p style="text-align: center;">CONFIDENTIAL <i>Restricted to SIGMA scientific partners and members of the consortium, please do not pass around</i></p>	<p>Ref : SIGMA-2013-D2-72 Version : 01</p> <hr/> <p>Date :15 may Page : 3</p>
--	--	---

INDEX

1.	INTRODUCTION.....	4
2.	DBN2 DATASET	5
3.	GROUND MOTION PREDICTION EQUATIONS	11
3.1.	DATASET	11
3.2.	FUNCTIONAL FORM	12
3.3.	DETERMINATION OF COEFFICIENTS.....	14
3.4.	RESULTS.....	21
4.	ANALYSIS OF RESIDUALS.....	30
4.1.	STANDARD DEVIATIONS	30
4.1.	DECOMPOSITION OF THE RESIDUALS	31
5.	CONCLUSIONS	40
6.	REFERENCE.....	42

	<p>Research and Development Programme on Seismic Ground Motion</p> <p>CONFIDENTIAL <i>Restricted to SIGMA scientific partners and members of the consortium, please do not pass around</i></p>	<p>Ref : SIGMA-2013-D2-72 Version : 01</p> <hr/> <p>Date :15 may Page : 4</p>
--	--	---

1. Introduction


The 2012 Po plain seismic sequence data reveal new features of the observed ground shaking levels in the northern Italy, that were not taken into account in previous models for the paucity of instrumental observations. Therefore they represent an invaluable information source for ground motion studies in a poorly investigated area characterized by some peculiarities, as:

- a) **deep alluvial cover:** the Po plain is one of the largest sedimentary basins in the world with an area of about 50.000 km² and a sediment thickness varying from few tens of meters to about 8 km;
- b) **surface waves:** besides the amplification due to the soft surface layers, the basin structure may also trap the incoming seismic waves and convert the body waves into surface waves, thus prolonging the ground shaking within the basin (Hanks, 1975; Hisada et al., 1993; Sato et al. 1999; Joyner, 2000; Somerville et al., 2004; Kagawa et al., 2004);
- c) **thrust faults:** the Po Plain earthquakes may be ascribed to a thrust faults system. This characteristic is remarkable because, before the 2012, the Italian strong motion catalogue was mainly composed of records from earthquakes with normal focal mechanism recorded in the central-southern Apennines.

A previous work on the characteristic of the ground motion in northern Italy was performed in November 2012 (deliverable SIGMA-2012-D2-53_02, Pacor et al., 2012).

In that study, a first version of the northern Italy strong-motion dataset, DBN, was released including 1440 records from 224 stations, relative to seismic events from 1976 (Friuli sequence) to 2012 (Emilia sequence) in the magnitude range 3.5 – 6.4. This dataset was used to evaluate the performance of five GMPEs, based on global, European and Italian datasets in describing the ground motion in northern Italy and especially in the Po plain region.

In this work we compile a new version of the dataset, called DBN2, adding new records, mainly acquired by temporary stations and improving the metadata, with updated information relative to earthquakes and stations. Then, we exploit such improvements to extract qualified subsets of data for calibrating new GMPEs specific for northern Italy.

	<p>Research and Development Programme on Seismic Ground Motion</p> <p>CONFIDENTIAL <i>Restricted to SIGMA scientific partners and members of the consortium, please do not pass around</i></p>	<p>Ref : SIGMA-2013-D2-72 Version : 01</p> <p>Date :15 may Page : 5</p>
--	--	---

Several reasons motivate the development of such regional predictive equations: first of all, the limited number of past studies on ground motion attenuation for this area and the availability of high-quality data recorded on deep sediments both at short and intermediate distance from the epicenters, that have never been investigated in Italy. Then, the results on the performance of existing GMPEs to predict the ground motion in northern Italy showed that all the considered equations are not able to represent high-frequency motion, predicting values which are larger than the observations. Furthermore, the DBN dataset presents some peculiar features, that cannot be reproduced by any GMPEs that are: i) low amplitudes at short periods, ii) attenuation with distance strongly dependent on frequency; iii) amplification of spectral ordinates in the distance range from 80 to 100km, particularly evident at short periods (0.1 s).

This deliverable is organized as follows. First, the updated version of DBN is presented and the data-sets used to derive regional GMPEs are described. Then, the calibrated models are discussed in terms of average models. Finally, the analysis on residuals is reported, with the aim of recognizing which are the contributions of the variability associated to the GMPEs.

2. DBN2 DATASET

The first release of DBN (deliverable SIGMA-2012-D2-53_02, Pacor et al., 2012) has been updated (deliverable SIGMA0002, Pacor et al., 2013) with about 250 strong-motion data from the 2012 Emilia aftershocks with $M > 5.0$, recorded by temporary and permanent stations of the National Accelerometric Network (RAN, Rete Accelerometrica Nazionale), operated by the Italian Department of Civil Protection (DPC, Dipartimento della Protezione Civile). In addition, about 400 records from events with $M > 3.9$ recorded by INGV temporary stations (Figure 1) installed in the epicentral area shortly after the 2012 Emilia main-shock (20th May, $M_w = 6.1$) have been included.

The INGV temporary stations, denoted by T0 (20 sites), were installed with the aim of improving hypocentral locations of the events (Moretti et al., 2012). Moreover, two seismic arrays, indicated by CAS (8 strong-motion sites) and MIR (8 strong-motion sites), were located orthogonally to the Po river bed with the main goal of investigating the site response of the Po plain sediments (Bordoni et al., 2012). The CAS and MIR stations were installed along NW-SE and N-S directions, respectively, and sample different morphological features of the Po river alluvial basin (crevasses splays, fluvial ridges, alluvial fans and ancient riverbeds).

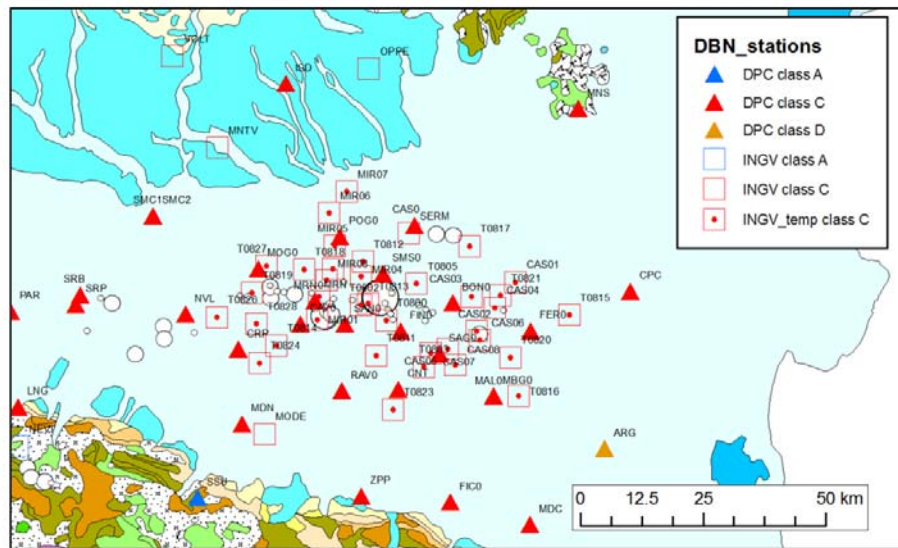
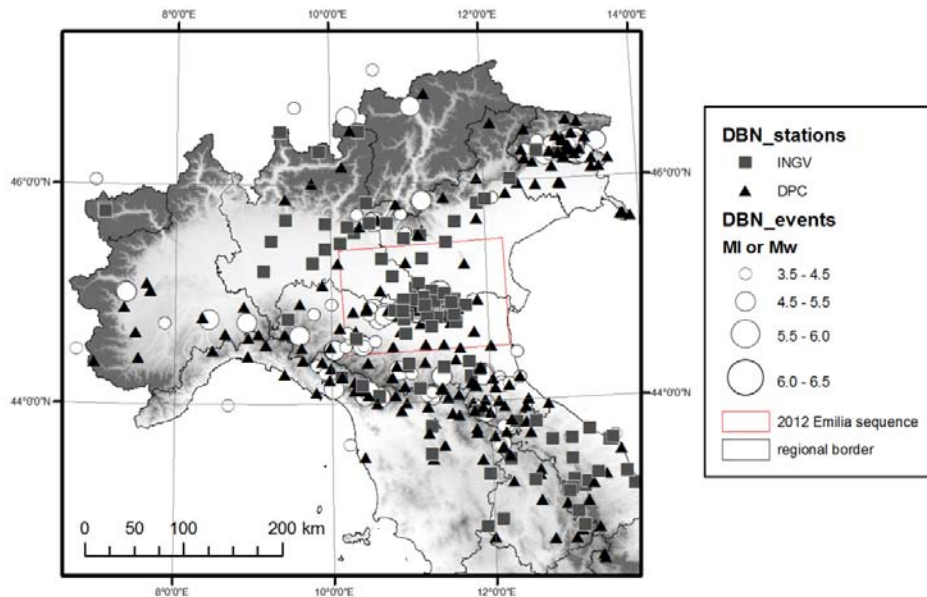



Figure 1a) Map of the epicenters (*white circles*) included in the DBN2 dataset together with the accelerometric stations. Black triangles: DPC stations; black squares: INGV stations; red box: epicentral area of the 2012 Emilia seismic sequence; black lines: regional borders. **b)** Zoom on the epicentral area of the 2012 Emilia sequence overlapped to the geological map (1:500.000 scale, Carta Geolomorfológica della Pianura Padana, 1997). Site classes (EC8, CEN 2004) are also reported. INGV temporary stations are classified as EC8 - C (CAS, MIR and T0) and are denoted by red squares with a dot. The geology of the Po plain is characterized by Pleistocene marine deposits overlapped by Holocene alluvial deposits. In the northern Apennines sandstones, marls, calcareous marls and chaotic deposits crop out.

	<p style="text-align: center;">Research and Development Programme on Seismic Ground Motion</p> <p style="text-align: center;">CONFIDENTIAL <i>Restricted to SIGMA scientific partners and members of the consortium, please do not pass around</i></p>	<p>Ref : SIGMA-2013-D2-72 Version : 01</p> <hr/> <p>Date : 15 may Page : 7</p>
--	--	--

In total, the updated version of DBN, hereinafter denominated DBN2, includes about 700 new accelerograms relative to events with $M > 3.9$, and the number of data at short epicentral distance is strongly increased with respect to DBN.

In order to improve the quality of the dataset, we performed a careful revision of available information and several events, stations and waveforms were removed. The following criteria have been followed to exclude records: stations not installed in free-field conditions (e.g. SMU, SMT, MAT and MAA, located in Friuli region); events with poor determination of magnitude and location; events not representative of the seismo-tectonic context of northern Italy (e.g. 1972 Ancona seismic sequence); records with probable instrumental bugs (i.e. malfunctioning of sensors; low-quality waveforms; noisy records). Furthermore, we carried out a preliminary residual analysis to identify waveforms, events and stations with the largest errors with respect to mean predictions, estimated by Bindi et al. (2011) GMPEs, hereinafter ITA10, valid for Italian territory.

Through this analysis we identified the strong motion data characterized by extremely high residuals ($R_{ij} > |2| \log_{10}$ unit), and removed them from DBN2.

The final release of the DBN2 strong-motion dataset is composed by 2174 waveforms, occurred in northern Italy [43°30'N - 46° 30'N latitude; 8°00'E - 13° 50'E longitude] in the period 1976 - 2012. The DBN2 includes 136 earthquakes (109 of them recorded by more than 1 stations) mainly located in the Tusco-Emiliano Apennines, the north-Eastern Italy and the Po Plain (Figure 1). The number of stations is 299 stations, 248 of them having more than 1 records.

In DBN2, earthquakes and stations metadata were reviewed according to the most reliable sources. Focal mechanisms and moment magnitudes (M_w) come from specific studies or the Regional Centroid Moment Tensor project (<http://www.bo.ingv.it/RCMT/> and Pondrelli et al., 2001; 2002; 2006; 2007; 2011).

Before 1982, locations and magnitudes of the major events are taken from literature (e.g., Slejko et al., 1999 for the 1976 Friuli seismic sequence), while locations and local magnitudes (M_l) of the events from 1982 to 2010 mainly come from the Italian Seismic Catalog For events from 1982 to 2010 (CSI 1.1, <http://csi.rm.ingv.it/> and Castello et al., 2006) or Bollettino Sismico Italiano (<http://bollettinosismico.rm.ingv.it/>). For the most recent earthquakes, after 2012, the metadata are derived from ISIDE catalogues (<http://iside.rm.ingv.it/>).

The recording stations were classified according to the average shear wave velocity of the uppermost 30 m, $V_{s,30}$ (EC8: Comité Européen de Normalisation, 2004), where the velocity of class A is larger than 800 m/s, B is in the range 360–800 m/s, C in the range 180–360 m/s, and D is lesser

than 180 m/s, E is characterized by 5-20 m of C or D-type alluvium underlain by stiffer material with $V_{S,30} \geq 800$ m/s (Di Capua et al., 2011; ITACA database, <http://itaca.mi.ingv.it>).

Stations without $V_{S,30}$ measurements, were classified revising the geological features on the base of geological maps (1:500.000 scale or 1:100.000 scale for uncertain locations) and their site classes is indicated adding an asterix.

In Figure 2, the distribution of magnitude versus distance for DBN2 dataset is displayed highlighting the records relative to the 2012 Emilia events and grouping the records on the base of the EC8 site-classes.

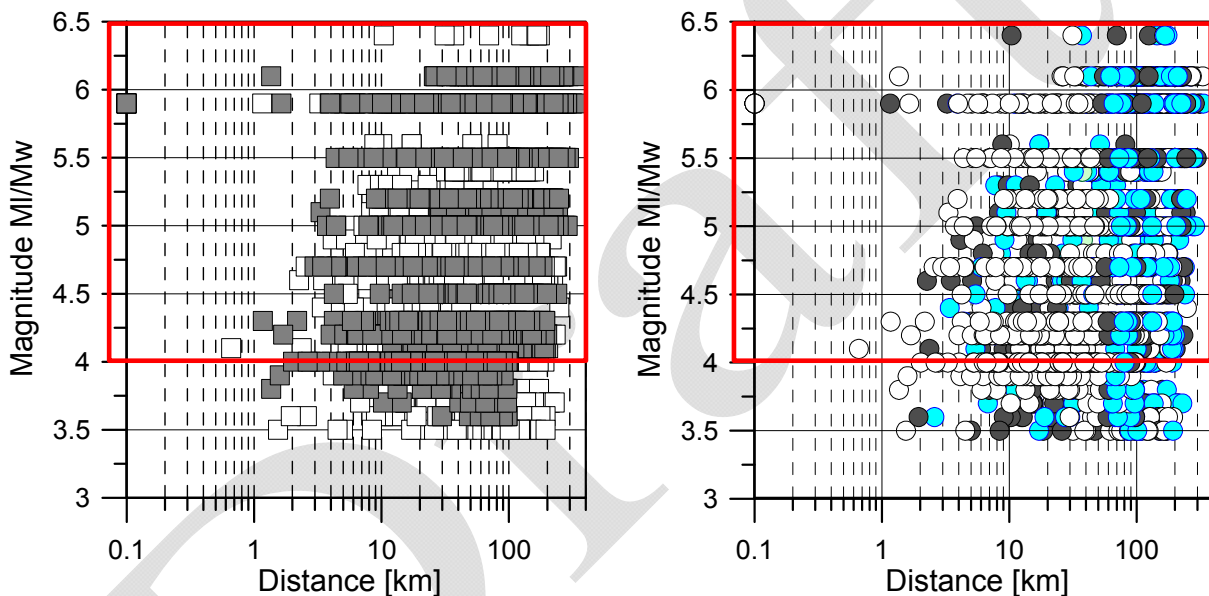


Figure 2. Magnitude-distance distribution for DBN2. The magnitude is M_w if available in DBN2, M_I otherwise; for the most of events with $M > 5.5$, the distance is Joyner and Boore distance; epicentral distance in the other cases. Left: records from the Emilia sequence are indicated by grey squares. Right: records are grouped according to EC8 site classes; EC8-A: blue, EC8-B: grey, EC8-C: white, EC8-D: yellow, EC8-E: green. The red frame indicates the dataset extracted for calibrating regional GMPEs.

The DBN2 magnitude (M_I or M_w) samples a magnitude range spanning from 3.5 – 6.4.

Note that two magnitude measurements are used: local magnitude (M_I) for small events (mainly with M_I between 3.5 and 4.5) and moment magnitude (M_w) for earthquakes with $M > 4.5$.

The most significant events belong to the 1976 Friuli (maximum magnitude M 6.4) and the 2012 Emilia sequences (maximum magnitude M 6.1). The latter provides a huge quantity of high quality strong-motion records and represents about the 2/3 of the entire dataset of northern Italy. The major

contribution in terms of records comes from the 4 strongest Emilia events recorded by more than 100 stations within 300 km from the epicenters (Table 1).

YYYYMMDDhhmmss	Lat	Lon	H [km]	M_w	# rec
20120603192043	44.90	10.94	9.2	5.0	124
20120529105557	44.89	11.01	6.8	5.5	144
20120520020352	44.89	11.23	6.3	6.1	168
20120529070003	44.85	11.09	10.2	5.9	195

Table 1. Earthquakes of the 2012 Emilia sequence characterized by more than 100 strong-motion data (#rec), recorded within 300 km.

In DBN2, two distance definitions are considered: the epicentral distance (R_{epi}), for $M < 5.5$ events, and the Joyner-Boore distance (R_{jb}) for which the fault geometry data is available in the DISS database (Working group, 2010) or after GPS studies.

The maximum distance range covered by DBN2 dataset is 300 km. The records are well sampled in the distance range from 10 to 150 km and in the magnitude range 3.5 – 5.5. About 30 records with distance $R_{jb} < 10$ km are available for $M_w > 5.5$, almost all relative to the three largest events of the Emilia sequence.

Figure 3 shows the distributions of distance (epicentral or Joyner and Boore distance) and magnitude (M_l or M_w) for DBN2. Note that all events with $M > 5.5$ are characterized by moment magnitude.

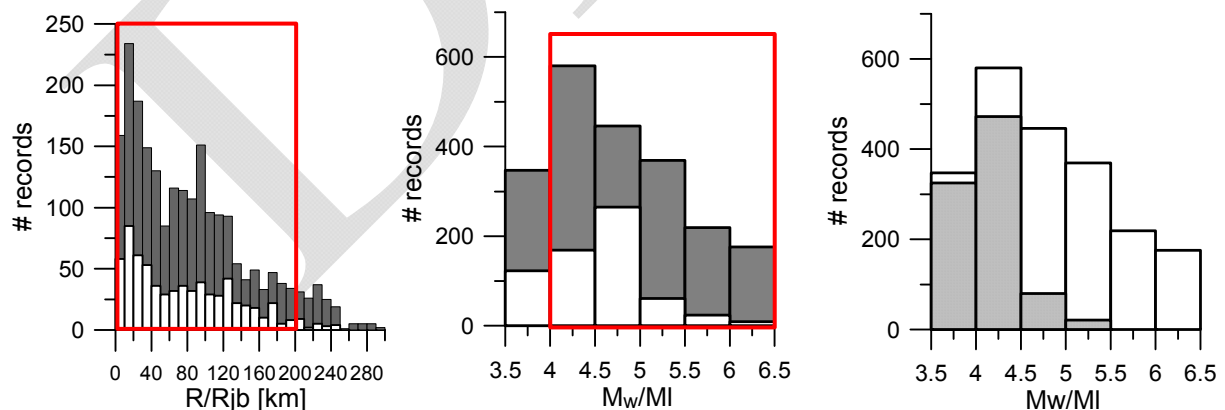


Figure 3. Distance (Left) and Magnitude (centre) distributions of the records included in the DBN2. Grey bars indicate the number of strong-motion records relative to the 2012 Emilia seismic sequence. Right: Local (light grey) and Moment magnitude (white) distributions for records of DBN2. The red frame indicates the dataset extracted for calibrating GMPEs.

Figure 4 shows the distribution of hypocentral depths, styles of faulting and site classes according to the EC8-site classification. The DBN2 records mainly come from superficial seismic sources, in the uppermost 15 km of the crust and the prevalent focal mechanism is thrust fault. The maximum hypocentral depth reaches 70 km.

After metadata revision, the number of records with associated unknown focal mechanism decreases, with respect to DBN, from about 400 to 100.

The better-sampled soil categories are EC8-C/C* (131 sites and 1123 records) and EC8-A/A* (95 sites and 610 records).

More than 60 stations (411 records) are in EC8-B/B* class and very few stations belong to EC8-D (2 sites and 10 records) and EC8-E (2 sites and 17 records) classes. Although a predominance of class C is evident (Figure 4), it is worth to notice that a number of stations classified as C* are located in the middle of the Po plain (Figure 1) where 2D and 3D basin effects could strongly affect the response site. Finally, it is important to note that the majority of the sites have been classified according to a geological description and only for about 35 sites, quantitative measures of $V_{S,30}$ are available.

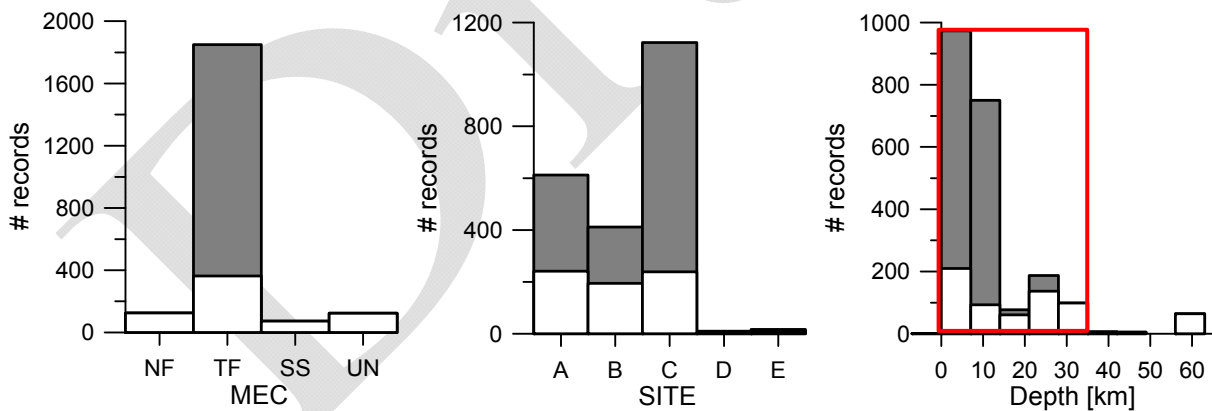



Figure 4. Focal mechanisms (*left*), EC8-site categories(*centre*)and hypocentral depths distributions of records included in DBN2. Grey bars indicate the number of strong-motion records relative to the 2012 Emilia seismic sequence. NF: Normal fault; TF: thrust fault; SS: Strike fault; UN: unknown mechanisms. The red frame indicates the dataset extracted for calibrating GMPEs

To derive the strong-ground motion parameters, the DBN2 records were uniformly processed using the ITACA procedure (Pacor et al., 2012) and summarized by the following steps: (1) baseline correction; (2) application of a cosine taper, based on the visual inspection of the record (typically

	<p>Research and Development Programme on Seismic Ground Motion</p> <p>CONFIDENTIAL <i>Restricted to SIGMA scientific partners and members of the consortium, please do not pass around</i></p>	<p>Ref : SIGMA-2013-D2-72 Version : 01</p> <p>Date :15 may Page : 11</p>
--	--	--

between 2 and 5% of the total record length); records identified as late-triggered are not tapered; (3) visual inspection of the Fourier spectrum to select the band-pass frequency range; (4) application of a 2nd order a-causal time-domain Butterworth filter to the acceleration time-series padded with zeros; (5) double-integration to obtain displacement time series; (6) linear de-trending of displacement and (7) double differentiation to get the corrected acceleration.

3. Ground Motion Prediction Equations

3.1. Dataset

The GMPEs for northern Italy are evaluated using two accelerometric data sets, extracted by DBN2.

- 1) *Dataset DBN2_A*. This dataset has been obtained selecting records in the magnitude range 4 - 6.4, where the local magnitudes have been converted into moment magnitudes using the relation proposed by Castello et al (2007). Four styles of faulting have been accounted for (NF, TF, SS, UN), as well as four site classes (A, B,C, C1), where C1 and C are EC8-C class located inside or the at the border (or outside) the Po plain, respectively. The distance (Joyner and Boore distance or epicentral distance) is in the range 0-200km and the event depth is lower than 30km. Furthermore, recordings have been considered such that each station should be present in the dataset with more than 2 recordings. No selection was done on number of records per earthquake, since this choice would have reduced the number of events with fault mechanisms other than thrust mechanism.

This data set is composed of 1701 records from 102 earthquakes and 178 stations.

- 2) *Dataset DBN2_B*. This dataset include same magnitude, distance and depth selection as *DBN2_A* and the same site and style of faulting classes. The difference is that local magnitudes have not been converted into moment magnitudes.

The data set is composed of 1539 records from 79 earthquakes and 173 stations.

The consequence of the conversion between local and moment magnitude implies that the total number of records in DBN2_A is larger than DBN2_B. This is because events with local magnitude between 3.6 and 3.9 are included, since, after the conversion, magnitude is > 4 .

The site classes D and E have not been considered since these categories are very poorly represented within DBN2 database (Figure 4).

The introduction of the C1 class is based on the observations that the waveforms relative to sites located in the middle of the basin have uncommon features compared with the EC8-C class strong-motion recordings, due to the relevant, and in many cases dominant, presence of surface waves. The near-source records are particularly complex, because of the superposition of body and surface waves with the latter having the largest amplitudes, while at more distant sites velocities and displacements generally occur in correspondence with the surface waves and an extreme lengthening of the signals can be observed (Luzi et al., 2013).

The distribution of records for site classes and focal mechanisms of the two datasets is reported in Table 2.

	Site A	Site B	Site C	Site C1	NF	TF	SS	UN
DBN2_A	429	279	317	676	55	1519	59	68
DBN2_B	377	245	286	631	54	1411	56	18

Table 2. Number of records per soil and style of faulting categories for the 2 considered datasets. NF: Normal fault; TF: thrust fault; SS: Strike fault; UN: unknown mechanisms.


3.2. Functional form

The GMPEs are derived considering a parametric model based on the following functional form (e.g. Bindi et al., 2011):

$$\log_{10} Y = e_1 + F_D(R, M) + F_M(M) + F_S + F_{sof} \quad [1]$$

where the distance F_D and magnitude F_M functional forms are given by:

$$F_D(R, M) = [c_1 + c_2(M - M_{ref})] \log_{10} \left(\sqrt{R_{JB}^2 + h^2} / R_{ref} \right) - c_3 \left(\sqrt{R_{JB}^2 + h^2} - R_{ref} \right) \quad [2]$$

	<p>Research and Development Programme on Seismic Ground Motion</p> <p>CONFIDENTIAL <i>Restricted to SIGMA scientific partners and members of the consortium, please do not pass around</i></p>	<p>Ref : SIGMA-2013-D2-72 Version : 01</p> <p>Date : 15 may Page : 13</p>
--	--	---

$$F_M(M) = \begin{cases} b_1(M - M_h) + b_2(M - M_h)^2 & \text{for } M \leq M_h \\ b_3(M - M_h) & \text{otherwise} \end{cases} \quad [3]$$

The explanatory variable M is magnitude, R (in km) is the Joyner and Boore distance when available and epicentral distance otherwise. For DBN2_B, we also calibrated regression coefficients using as metric the hypocentral distance. In this case, the pseudo-distance h is set equal to 0. We identify this case as DBN2_BH.

The functional form F_S in equation (1) represents the site amplification and it is given by $F_S = s_j C_j$, for $j=1, \dots, 4$, where s_j are the coefficients to be determined through the regression analysis, while C_j are dummy variables used to denote the four considered site classes: EC8-A, EC8-B, EC8-C and EC8-C1, that corresponds to EC8-C sites located on deep sediments.

The functional form F_{sof} in equation (1) represents the style of faulting correction and it is given by $F_{\text{sof}} = f_j E_j$, for $j=1, \dots, 4$, where f_j are the coefficients to be determined during the analysis and E_j are dummy variables used to denote the different fault classes: normal (NF), reverse (TF), strike-slip (SS) and unspecified (UN).

The variables M_{ref} , M_h , R_{ref} (equations 2 and 3) have been fixed to 5.0, 6.75 and 1km, respectively, after trial regressions and after Bindi et al. (2011). M_{ref} was selected after analyzing the decay with distance of observed peak values at different magnitudes (deliverable SIGMA0002, Pacor et al., 2013).

As response variable Y , the peak ground acceleration (PGA in cm/s^2) is considered, along with 5% damped spectral absolute acceleration (S_a in cm/s^2) computed over 24 periods in the range 0.04 - 4s. The regressions are performed applying a random effect approach (Abrahamson and Youngs, 1992), considering the geometric mean of the recorded horizontal components, hereinafter GEOH, and the vertical one, hereinafter Z .

The random effect approach is applied to determine the between-events, the within-event components of variability (Al Atik et al., 2010).

The regressions are performed constraining to zero the site coefficient for class A (rock). Two constraints are applied on the style of faulting coefficients: the unspecified focal mechanism is set to 0 as well the average of coefficient for strike, normal and unknown fault mechanism, i.e. ($f_1 + f_2 + f_3 = 0$).

Coefficients c_3 has been constraint to zero, as the bump at 80 – 120 km observed in the distance decay of peak values (deliverable SIGMA0002, Pacor et al., 2013) caused unrealistic anelastic

attenuation coefficients. Coefficient b_3 has been constraint to zero as well, as the maximum magnitude in the data set is 6.4.

3.3. Determination of coefficients

The regression coefficients and standard deviations obtained for GeoH and Z are shown in Tables from 3 to 7 for DBN2_A, DBN2_B and DBN2_BH.

The trend of the style of faulting coefficients in function of the period is shown in Figures 5 for case DBN2_B.

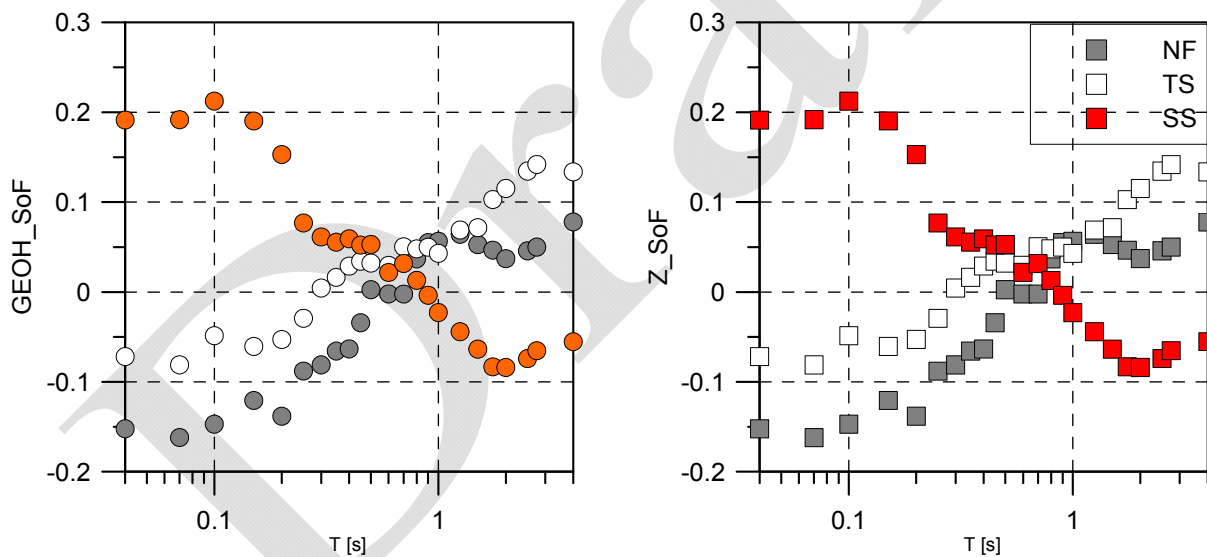


Figure 5. Focal mechanism coefficients obtained for GEOH for DBN2_B. Left: GEOH. Right: Z. DBN2_BH (bottom).

Style of faulting coefficients are generally small both for GEOH and Z: reverse faulting causes higher amplitudes at low periods (0 – 1s) than strike slip faulting and normal faulting.

The observed amplification relative to strike fault is not significant due to the scarce number of events for this category.

The trend of the site parameters in function of the period is shown in Figures 6. For comparison the coefficients for class C of the ITA10 GMPEs are also reported.

The site coefficients for GEOH show expected trends: site class B (i.e. stiff sites) amplifies the entire period range with an amplitude peak of 0.25 around 0.3s, class C moderately amplifies the long period range after 0.3s and class C1 causes a relevant amplification of long period ground motion, starting at 0.2s. At period larger than 0.6, the amplifications have the maximum values from 0.35 and 0.4 for cases DBN2_B and DBN2_BH.

For Z components, the B and C site-class coefficients are smaller than GEOH: they show an almost constant trend, with values around 0.15. Completely different is the trend of the C1 coefficients: these sites are characterized by significant de-amplification in the period range 0.2 – 1s, that could be due to high frequency attenuation properties of the deep sediments in the Po plain.

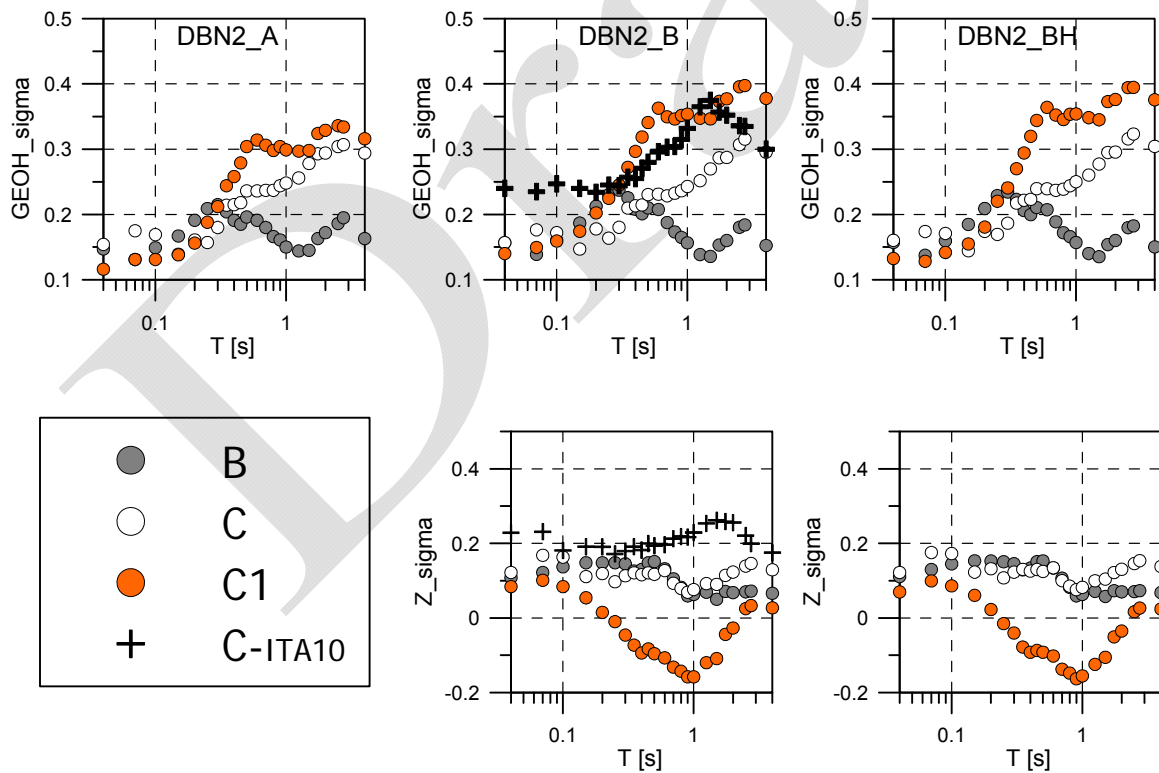


Figure 6. Site coefficients obtained for GEOH (top) for the three considered cases and Z (bottom) for DBN2_B and DBN2_BH.

T	a	b1	b2	c1	c2	h
0.04	3.4642	-0.2587	-0.1431	-1.652	0.2949	3.3857
0.07	3.9932	-0.1828	-0.1254	-1.8063	0.2618	5.7637
0.10	3.8749	-0.1401	-0.1308	-1.6593	0.2208	3.4286
0.15	4.2385	0.0092	-0.1303	-1.6722	0.1646	5.8223
0.20	4.1871	0.0395	-0.1403	-1.5981	0.1539	5.9365
0.25	4.1331	0.0084	-0.1574	-1.5962	0.162	6.5636
0.30	3.9726	-0.0407	-0.1712	-1.5758	0.1831	6.4275
0.35	4.0563	0.0444	-0.163	-1.5891	0.1636	7.2509
0.40	4.0384	0.0726	-0.1713	-1.5802	0.1478	7.7225
0.45	3.9803	0.1079	-0.1737	-1.5497	0.1385	7.762
0.50	3.9338	0.1433	-0.1715	-1.5248	0.1346	7.8482
0.60	3.801	0.1552	-0.186	-1.4774	0.1192	7.251
0.70	3.7247	0.2127	-0.1895	-1.4517	0.0955	7.1865
0.80	3.5905	0.1659	-0.1998	-1.4518	0.1238	7.9868
0.90	3.4693	0.1728	-0.1961	-1.4248	0.1379	7.7781
1.00	3.4333	0.1795	-0.1987	-1.429	0.1409	8.383
1.25	3.2868	0.1991	-0.2	-1.4107	0.1612	8.5265
1.50	3.2541	0.2704	-0.2001	-1.4151	0.1511	8.4693
1.75	3.2599	0.3651	-0.1916	-1.4141	0.1406	8.5419
2.00	3.2373	0.4447	-0.1787	-1.3953	0.1318	7.9307
2.50	3.1179	0.469	-0.171	-1.4251	0.1544	8.9985
2.75	3.0168	0.4946	-0.1636	-1.4254	0.1595	8.82
4.00	2.999	0.6684	-0.1134	-1.4723	0.1761	9.3359
PGA	3.6244	-0.1876	-0.1494	-1.6909	0.2637	5.7235

f1_NF	f2_TF	f3_SS	s2_B	s3_C	s4_C1	σbe	σwe	σtot
-0.0157	-0.17	0.0759	0.1821	0.1727	0.1361	0.2101	0.321	0.3837
-0.0334	-0.2004	0.0709	0.1593	0.1769	0.1183	0.2022	0.3503	0.4044
-0.0203	-0.1724	0.1145	0.182	0.1874	0.1516	0.2146	0.3718	0.4293
0.0099	-0.1635	0.0665	0.2054	0.1511	0.1475	0.2188	0.3553	0.4173
-0.0049	-0.1642	0.0421	0.2279	0.175	0.1681	0.2315	0.3336	0.406
0.0212	-0.1377	0.0091	0.2431	0.1685	0.1973	0.2306	0.3143	0.3898
0.0621	-0.1028	0.015	0.2477	0.1895	0.2201	0.222	0.3026	0.3753
0.064	-0.0822	0.0282	0.2345	0.2179	0.2449	0.2309	0.2981	0.377
0.0683	-0.0539	0.0439	0.2212	0.2219	0.266	0.2233	0.2883	0.3646
0.092	-0.0335	0.0423	0.213	0.2253	0.285	0.2354	0.2884	0.3723
0.1023	-0.0313	0.0309	0.2243	0.2436	0.3095	0.2349	0.2876	0.3713
0.1377	-0.003	0.0329	0.2174	0.2429	0.3206	0.2336	0.286	0.3693
0.1667	0.0383	0.0332	0.2018	0.24	0.3055	0.2317	0.2838	0.3664
0.1756	0.0348	0.02	0.1875	0.241	0.2975	0.2223	0.2869	0.363
0.1838	0.0437	0.0196	0.1817	0.247	0.3042	0.2334	0.2858	0.369
0.1881	0.0479	0.0189	0.173	0.252	0.302	0.2335	0.2859	0.3691
0.1743	0.0461	-0.0194	0.1616	0.2598	0.2968	0.2415	0.2809	0.3704
0.1989	0.0626	-0.0176	0.16	0.279	0.2926	0.2415	0.2808	0.3704
0.1983	0.0544	-0.0213	0.1769	0.2949	0.3155	0.2336	0.2861	0.3693
0.2045	0.0619	-0.0108	0.1815	0.2922	0.3184	0.2328	0.2851	0.3681
0.2017	0.0582	-0.0202	0.202	0.3055	0.3317	0.2361	0.2892	0.3734
0.1943	0.0646	-0.0116	0.2076	0.3122	0.3324	0.236	0.289	0.3731
0.178	0.0454	-0.0211	0.1785	0.294	0.3133	0.2327	0.285	0.368
-0.0002	-0.16	0.0591	0.203	0.1658	0.1443	0.216	0.3112	0.3788

Table 3- DBN2_A:Regression coefficients for absolute acceleration response spectra (see equations from 1 to 3) obtained for the geometrical mean of the horizontal components (GeoH).

T	a	b1	b2	c1	c2	h
0.04	3.7407	-0.0019	-0.0502	-1.7135	0.2431	5.9396
0.07	3.8175	0.0036	-0.0440	-1.6950	0.2295	4.2449
0.10	3.8232	-0.0523	-0.0574	-1.6817	0.2296	4.8246
0.15	3.9210	0.0640	-0.0540	-1.5901	0.1894	4.5575
0.20	3.7949	0.0868	-0.0634	-1.4868	0.1789	3.7264
0.25	4.0006	0.1354	-0.0603	-1.5738	0.1765	6.8655
0.30	4.0348	0.1980	-0.0499	-1.5833	0.1750	7.4530
0.35	4.0967	0.2550	-0.0448	-1.6022	0.1635	8.4328
0.40	4.1263	0.3275	-0.0403	-1.5953	0.1425	9.0136
0.45	4.0647	0.3743	-0.0394	-1.5576	0.1303	9.0221
0.50	4.0200	0.4118	-0.0395	-1.5250	0.1189	8.7606
0.60	3.9630	0.4706	-0.0394	-1.4872	0.1007	8.9523
0.70	3.9117	0.5361	-0.0422	-1.4606	0.0720	8.8580
0.80	3.7410	0.4993	-0.0468	-1.4426	0.1004	9.2432
0.90	3.6463	0.5121	-0.0428	-1.4189	0.1103	9.1719
1.00	3.5519	0.5131	-0.0427	-1.4040	0.1191	9.3916
1.25	3.4016	0.5701	-0.0335	-1.3767	0.1323	9.3759
1.50	3.3760	0.6455	-0.0292	-1.3818	0.1246	9.4532
1.75	3.4529	0.7967	-0.0134	-1.3793	0.0951	9.3553
2.00	3.3263	0.7702	-0.0161	-1.3725	0.1146	9.4626
2.50	3.1793	0.8202	-0.0064	-1.3707	0.1250	9.5082
2.75	3.1204	0.8713	0.0047	-1.3753	0.1233	9.5399
4.00	2.9829	0.9696	0.0377	-1.4070	0.1519	9.6507
PGA	3.3637	-0.0315	-0.0627	-1.5610	0.2461	3.6924

f1_NF	f2_TF	f3_SS	s2_B	s3_C	s4_C1	σbe	σwe	σtot
-0.0987	-0.0819	0.1379	0.1566	0.1568	0.1401	0.1747	0.3243	0.3684
-0.0693	-0.0959	0.1498	0.1388	0.1764	0.1494	0.1755	0.3510	0.3924
-0.0905	-0.0699	0.1875	0.1603	0.1720	0.1592	0.1861	0.3722	0.4161
-0.0550	-0.0678	0.1332	0.1868	0.1469	0.1742	0.1811	0.3623	0.4050
-0.0638	-0.0618	0.1147	0.2126	0.1778	0.2023	0.1836	0.3407	0.3870
-0.0672	-0.0439	0.0583	0.2303	0.1636	0.2247	0.1740	0.3229	0.3668
-0.0519	-0.0282	0.0320	0.2372	0.1803	0.2452	0.1561	0.3121	0.3490
-0.0569	-0.0127	0.0423	0.2257	0.2098	0.2722	0.1540	0.3079	0.3443
-0.0659	0.0096	0.0498	0.2079	0.2134	0.2966	0.1492	0.2983	0.3335
-0.0437	0.0311	0.0489	0.2011	0.2145	0.3187	0.1498	0.2997	0.3350
-0.0367	0.0311	0.0357	0.2101	0.2304	0.3409	0.1500	0.3000	0.3354
-0.0290	0.0366	0.0122	0.2076	0.2311	0.3629	0.1497	0.2993	0.3347
-0.0163	0.0662	-0.0001	0.1875	0.2286	0.3496	0.1483	0.2966	0.3316
-0.0099	0.0649	-0.0127	0.1733	0.2325	0.3463	0.1493	0.2986	0.3339
-0.0120	0.0665	-0.0225	0.1648	0.2363	0.3516	0.1494	0.2988	0.3341
-0.0065	0.0739	-0.0257	0.1565	0.2428	0.3537	0.1493	0.2986	0.3339
-0.0080	0.0960	-0.0392	0.1385	0.2517	0.3475	0.1476	0.2951	0.3300
0.0016	0.1043	-0.0455	0.1356	0.2698	0.3464	0.1476	0.2951	0.3300
0.0026	0.0967	-0.0474	0.1531	0.2868	0.3733	0.1387	0.3012	0.3316
0.0014	0.1018	-0.0408	0.1600	0.2873	0.3772	0.1392	0.3021	0.3326
0.0034	0.1014	-0.0458	0.1803	0.3070	0.3956	0.1408	0.3057	0.3366
-0.0044	0.1055	-0.0421	0.1839	0.3154	0.3975	0.1413	0.3067	0.3377
-0.0012	0.1015	-0.0316	0.1524	0.2954	0.3779	0.1387	0.3011	0.3315
-0.0623	-0.0645	0.1254	0.1811	0.1642	0.1798	0.1818	0.3149	0.3636

Table 4 - DBN2_B: Regression coefficients for absolute acceleration response spectra (see equations from 1 to 3) obtained for the geometrical mean of the horizontal components (GeoH).

T	a	b1	b2	c1	c2
0.04	4.2719	0.2151	-0.0203	-1.8102	0.2030
0.07	4.6669	0.3202	-0.0022	-1.8816	0.1602
0.10	4.7244	0.3417	-0.0039	-1.8463	0.1399
0.15	4.7321	0.3825	-0.0121	-1.7557	0.1187
0.20	4.6064	0.3790	-0.0252	-1.6719	0.1148
0.25	4.5485	0.4119	-0.0241	-1.6397	0.1145
0.30	4.4971	0.4351	-0.0219	-1.6293	0.1185
0.35	4.4594	0.4689	-0.0205	-1.6114	0.1125
0.40	4.4375	0.5209	-0.0217	-1.5879	0.0919
0.45	4.3751	0.5886	-0.0135	-1.5439	0.0816
0.50	4.3271	0.6234	-0.0121	-1.5159	0.0740
0.60	4.2684	0.6828	-0.0128	-1.4774	0.0538
0.70	4.1834	0.7264	-0.0177	-1.4497	0.0332
0.80	4.0999	0.7545	-0.0147	-1.4315	0.0400
0.90	3.9064	0.7069	-0.0179	-1.3999	0.0683
1.00	3.8108	0.7056	-0.0194	-1.3825	0.0753
1.25	3.6476	0.7562	-0.0104	-1.3555	0.0916
1.50	3.7639	0.9269	0.0072	-1.3700	0.0571
1.75	3.6755	0.9638	0.0072	-1.3599	0.0603
2.00	3.6278	0.9940	0.0130	-1.3557	0.0650
2.50	3.4622	1.0291	0.0195	-1.3523	0.0772
2.75	3.4139	1.0820	0.0297	-1.3587	0.0726
4.00	3.3069	1.2076	0.0664	-1.3868	0.0937
PGA	4.1757	0.2424	-0.0274	-1.7566	0.1860

f1_NF	f2_TF	f3_SS	s2_B	s3_C	s4_C1	σbe	σwe	σtot
-0.1647	-0.1257	0.2022	0.1570	0.1603	0.1324	0.1652	0.3305	0.3695
-0.1485	-0.1457	0.2088	0.1374	0.1739	0.1282	0.1782	0.3565	0.3985
-0.1629	-0.1218	0.2424	0.1594	0.1709	0.1418	0.1595	0.3797	0.4118
-0.1294	-0.1190	0.1846	0.1847	0.1443	0.1548	0.1834	0.3669	0.4102
-0.1376	-0.1087	0.1653	0.2091	0.1740	0.1806	0.1730	0.3460	0.3869
-0.1197	-0.0869	0.1141	0.2289	0.1694	0.2202	0.1635	0.3270	0.3656
-0.0976	-0.0656	0.0953	0.2344	0.1865	0.2407	0.1574	0.3148	0.3520
-0.1015	-0.0514	0.1054	0.2230	0.2173	0.2701	0.1548	0.3095	0.3461
-0.1052	-0.0269	0.1152	0.2060	0.2218	0.2942	0.1495	0.2990	0.3343
-0.0862	-0.0071	0.1073	0.1997	0.2231	0.3198	0.1507	0.3014	0.3370
-0.0782	-0.0054	0.0917	0.2106	0.2395	0.3440	0.1507	0.3014	0.3369
-0.0656	0.0043	0.0708	0.2073	0.2393	0.3640	0.1503	0.3007	0.3362
-0.0520	0.0343	0.0557	0.1887	0.2370	0.3523	0.1495	0.2989	0.3342
-0.0449	0.0324	0.0429	0.1719	0.2387	0.3453	0.1497	0.2995	0.3348
-0.0468	0.0358	0.0323	0.1659	0.2440	0.3536	0.1496	0.2992	0.3345
-0.0435	0.0412	0.0278	0.1570	0.2502	0.3541	0.1494	0.2989	0.3341
-0.0429	0.0652	0.0149	0.1402	0.2603	0.3483	0.1475	0.2949	0.3297
-0.0339	0.0702	0.0041	0.1352	0.2773	0.3451	0.1247	0.2968	0.3219
-0.0309	0.0692	0.0095	0.1538	0.2950	0.3729	0.1266	0.3014	0.3269
-0.0355	0.0691	0.0101	0.1601	0.2956	0.3761	0.1268	0.3018	0.3274
-0.0334	0.0693	0.0063	0.1798	0.3158	0.3943	0.1282	0.3052	0.3310
-0.0417	0.0736	0.0108	0.1825	0.3233	0.3947	0.1285	0.3059	0.3318
-0.0399	0.0661	0.0205	0.1502	0.3043	0.3757	0.1263	0.3007	0.3262
-0.1403	-0.1121	0.1812	0.1787	0.1598	0.1555	0.1609	0.3219	0.3599

Table 5 - DBN2_BH: Regression coefficients for absolute acceleration response spectra (see equations from 1 to 3) obtained for the geometrical mean of the horizontal components (GeoH).

T	a	b1	b2	c1	c2	h
0.04	4.294	0.302	-0.0137	-1.900	0.1320	5.084
0.07	4.730	0.428	-0.0219	-1.909	0.0348	6.301
0.10	4.758	0.511	-0.0079	-1.843	0.0146	7.563
0.15	4.700	0.533	-0.0102	-1.754	0.0148	8.836
0.20	4.523	0.441	-0.0349	-1.715	0.0462	9.304
0.25	4.291	0.400	-0.0353	-1.650	0.0787	9.465
0.30	4.101	0.390	-0.0361	-1.597	0.0936	9.571
0.35	4.115	0.475	-0.0197	-1.580	0.0844	9.561
0.40	4.081	0.551	-0.0106	-1.540	0.0756	9.449
0.45	3.915	0.545	-0.0099	-1.495	0.0968	9.417
0.50	3.862	0.572	-0.0045	-1.473	0.1022	9.447
0.60	3.803	0.626	-0.0091	-1.419	0.0716	9.203
0.70	3.529	0.546	-0.0270	-1.364	0.1014	9.297
0.80	3.401	0.554	-0.0345	-1.312	0.1000	9.117
0.90	3.339	0.546	-0.0334	-1.310	0.1131	9.340
1.00	3.250	0.548	-0.0336	-1.291	0.1213	8.915
1.25	3.110	0.587	-0.0245	-1.289	0.1452	8.427
1.50	3.110	0.605	-0.0298	-1.333	0.1518	9.061
1.75	3.145	0.711	-0.0190	-1.358	0.1371	9.365
2.00	3.167	0.787	-0.0017	-1.372	0.1419	9.378
2.50	2.985	0.833	0.0066	-1.345	0.1578	9.570
2.75	2.891	0.836	0.0001	-1.340	0.1567	9.716
4.00	2.804	0.992	0.0275	-1.319	0.1652	9.821
PGA	4.069	0.362	-0.0148	-1.776	0.1167	6.145


f1_NF	f2_TF	f3_SS	s2_B	s3_C	s4_C1	σbe	σwe	σtot
-0.1522	-0.0719	0.1913	0.108	0.122	0.084	0.168	0.313	0.355
-0.1619	-0.0811	0.1917	0.122	0.168	0.101	0.177	0.329	0.374
-0.1471	-0.0486	0.2124	0.137	0.163	0.084	0.153	0.333	0.366
-0.1207	-0.0606	0.1903	0.148	0.111	0.054	0.172	0.319	0.363
-0.1382	-0.0528	0.1529	0.148	0.119	0.015	0.186	0.303	0.356
-0.0880	-0.0293	0.0768	0.148	0.097	-0.010	0.186	0.284	0.340
-0.0811	0.0044	0.0612	0.145	0.113	-0.046	0.174	0.282	0.331
-0.0657	0.0163	0.0554	0.126	0.121	-0.073	0.171	0.279	0.327
-0.0633	0.0288	0.0592	0.130	0.116	-0.094	0.181	0.277	0.331
-0.0342	0.0342	0.0522	0.148	0.121	-0.083	0.189	0.272	0.331
0.0026	0.0322	0.0529	0.151	0.117	-0.096	0.197	0.268	0.333
-0.0022	0.0297	0.0218	0.132	0.127	-0.107	0.204	0.264	0.334
-0.0023	0.0503	0.0317	0.105	0.093	-0.132	0.215	0.264	0.340
0.0369	0.0480	0.0130	0.082	0.079	-0.143	0.206	0.265	0.336
0.0550	0.0499	-0.0037	0.059	0.069	-0.158	0.215	0.264	0.341
0.0565	0.0430	-0.0229	0.063	0.076	-0.158	0.205	0.265	0.335
0.0642	0.0689	-0.0442	0.069	0.092	-0.120	0.201	0.273	0.339
0.0527	0.0716	-0.0636	0.050	0.090	-0.109	0.207	0.282	0.350
0.0466	0.1029	-0.0832	0.071	0.114	-0.044	0.209	0.285	0.354
0.0371	0.1152	-0.0840	0.068	0.123	-0.027	0.212	0.290	0.3599
0.0458	0.1345	-0.0741	0.070	0.139	0.025	0.209	0.301	0.3672
0.0500	0.1419	-0.0653	0.072	0.146	0.033	0.219	0.298	0.3706
0.0780	0.1337	-0.0553	0.066	0.129	0.027	0.214	0.309	0.3761
-0.1491	-0.0449	0.1759	0.116	0.093	0.020	0.167	0.289	0.3346

Table 6 - DBN2_B: Regression coefficients for absolute acceleration response spectra (see equations from 1 to 3) obtained for the geometrical mean of the vertical components (Z).

T	a	b1	b2	c1	c2
0.04	5.1300	0.6446	0.0314	-2.0607	0.0592
0.07	5.4178	0.7672	0.0246	-2.0073	-0.0337
0.10	5.2808	0.8103	0.0326	-1.8846	-0.0457
0.15	5.0739	0.7992	0.0254	-1.7435	-0.0395
0.20	4.8918	0.7263	0.0029	-1.6862	-0.0160
0.25	4.6895	0.7011	0.0029	-1.6249	0.0081
0.30	4.4661	0.6648	-0.0019	-1.5704	0.0296
0.35	4.4502	0.7267	0.0118	-1.5537	0.0267
0.40	4.3072	0.7292	0.0115	-1.5111	0.0403
0.45	4.2038	0.7591	0.0170	-1.4746	0.0498
0.50	4.1804	0.8008	0.0241	-1.4558	0.0503
0.60	4.0692	0.8104	0.0131	-1.4090	0.0309
0.70	3.7847	0.7290	-0.0040	-1.3511	0.0625
0.80	3.6932	0.7519	-0.0099	-1.3095	0.0557
0.90	3.6320	0.7494	-0.0088	-1.3010	0.0656
1.00	3.5426	0.7357	-0.0110	-1.2913	0.0779
1.25	3.4161	0.7717	-0.0003	-1.3034	0.1075
1.50	3.3901	0.7997	-0.0043	-1.3306	0.1109
1.75	3.4038	0.8851	0.0023	-1.3514	0.0999
2.00	3.4392	0.9694	0.0202	-1.3661	0.1013
2.50	3.3558	1.0843	0.0377	-1.3436	0.0976
2.75	3.2179	1.0658	0.0284	-1.3295	0.1019
4.00	3.1075	1.2145	0.0549	-1.3003	0.1124
PGA	4.6668	0.6265	0.0201	-1.8734	0.0635

f1_NF	f2_TF	f3_SS	s2_B	s3_C	s4_C1	σbe	σwe	σtot
-0.2290	-0.1234	0.2580	0.1109	0.1220	0.0696	0.1620	0.3240	0.3622
-0.2208	-0.1233	0.2599	0.1297	0.1755	0.0992	0.1681	0.3362	0.3759
-0.1959	-0.0879	0.2800	0.1448	0.1725	0.0859	0.1682	0.3365	0.3762
-0.1631	-0.0996	0.2538	0.1532	0.1229	0.0605	0.1848	0.3202	0.3697
-0.1803	-0.0959	0.2109	0.1528	0.1320	0.0225	0.2000	0.3055	0.3652
-0.1301	-0.0716	0.1333	0.1506	0.1074	-0.0153	0.1876	0.2865	0.3425
-0.1256	-0.0388	0.1145	0.1455	0.1228	-0.0405	0.1637	0.2835	0.3273
-0.1107	-0.0258	0.1088	0.1286	0.1302	-0.0781	0.1618	0.2803	0.3236
-0.1046	-0.0072	0.1168	0.1336	0.1256	-0.0920	0.1604	0.2778	0.3208
-0.0745	-0.0011	0.1074	0.1509	0.1300	-0.0871	0.1786	0.2728	0.3260
-0.0408	-0.0061	0.1038	0.1530	0.1247	-0.0919	0.1758	0.2685	0.3209
-0.0362	0.0019	0.0802	0.1338	0.1344	-0.1021	0.1931	0.2632	0.3264
-0.0404	0.0190	0.0821	0.1066	0.1000	-0.1376	0.2137	0.2617	0.3379
0.0044	0.0218	0.0670	0.0821	0.0852	-0.1479	0.1935	0.2636	0.3270
0.0188	0.0196	0.0465	0.0591	0.0757	-0.1632	0.1930	0.2630	0.3263
0.0199	0.0133	0.0275	0.0631	0.0820	-0.1554	0.1943	0.2648	0.3284
0.0271	0.0403	0.0069	0.0712	0.0997	-0.1245	0.1786	0.2729	0.3261
0.0199	0.0448	-0.0107	0.0577	0.1041	-0.1057	0.1836	0.2805	0.3352
0.0083	0.0745	-0.0270	0.0730	0.1218	-0.0509	0.1849	0.2824	0.3376
-0.0019	0.0862	-0.0280	0.0700	0.1304	-0.0352	0.1879	0.2870	0.3431
0.0049	0.1014	-0.0238	0.0704	0.1457	0.0166	0.1725	0.2988	0.3450
0.0100	0.1092	-0.0150	0.0732	0.1537	0.0265	0.1939	0.2962	0.3540
0.0351	0.0959	-0.0109	0.0680	0.1379	0.0240	0.2010	0.3071	0.3670
-0.2087	-0.0873	0.2414	0.1216	0.0983	0.0144	0.1714	0.2968	0.3427

Table 7 - DBN2_BH: Regression coefficients for absolute acceleration response spectra (see equations from 1 to 3) obtained for the geometrical mean of the vertical components (Z).

	<p>Research and Development Programme on Seismic Ground Motion</p> <p>CONFIDENTIAL <i>Restricted to SIGMA scientific partners and members of the consortium, please do not pass around</i></p>	<p>Ref : SIGMA-2013-D2-72 Version : 01</p> <p>Date : 15 may Page : 21</p>
--	--	---

3.4. Results

In Figures 7 to 10, the PGA and spectral ordinates S_a at periods 0.3s, 1s and 4s, for GEOH and 2s for Z, predicted by the GMPE developed in this study (DBN2_B) are compared to the observations relative to A and C1 soil classes for thrust events and magnitude 5 and 6. The predictions of DBN2_B are also compared with ITA10. For ITA10, C and A site classes are considered.

On average, the predictions match reasonably well the observations over the entire distance range, for all periods, both for class A and C1.

However it is important to note that class A sites included in DBN2 are almost all located at large distances from the epicenter ($R > 80\text{km}$). As consequence, for these sites, the model is not constrained close to the seismic sources (Figures 7b, 8b, 9b and 10b).

At magnitude 6, for C1 sites located over the fault, plotted at $R_{JB} = 0.1\text{ km}$ in Figures 7a and 8a, good agreement is observed between the predicted spectral acceleration level and recorded data both for GEOH and Z components, especially at long periods. On the contrary, the predicted PGA are larger than the observations for GEOH.

At magnitude 5, the median model well describes observed data for distances larger than 10km for class C1. In the distance range between 1 and 10 km, the observations are more scattered (Figure 9a and 10a).

When we compare the ITA10 and DBN2_B GMPEs, we observe that the mean predictions and associated errors are very similar at intermediate periods (0.3 – 1 s) and distance larger than 10 km for both considered magnitudes.

At long periods ($T > 2\text{s}$), for GEOH and soft sites (Figures 7a and 9a) DBN2_B predicts larger mean values than ITA10 up to 100 km, caused by the low frequency amplification of the C1 soil class.

On the contrary, at $T = 1\text{s}$ for Z component and soft sites (class C1), the ITA10 mean curve strongly overestimates the DBN2_B mean predictions (Figures 8a and 10a). This is caused by the strong attenuation up to 1 Hz, as described by C1 site coefficient (Figure 6).

Finally we observe that for PGA and all cases, the ITA10 median predictions are lower than DBN2_B at distances smaller than 10 km and they show weaker attenuation with distance, especially for C1 sites.

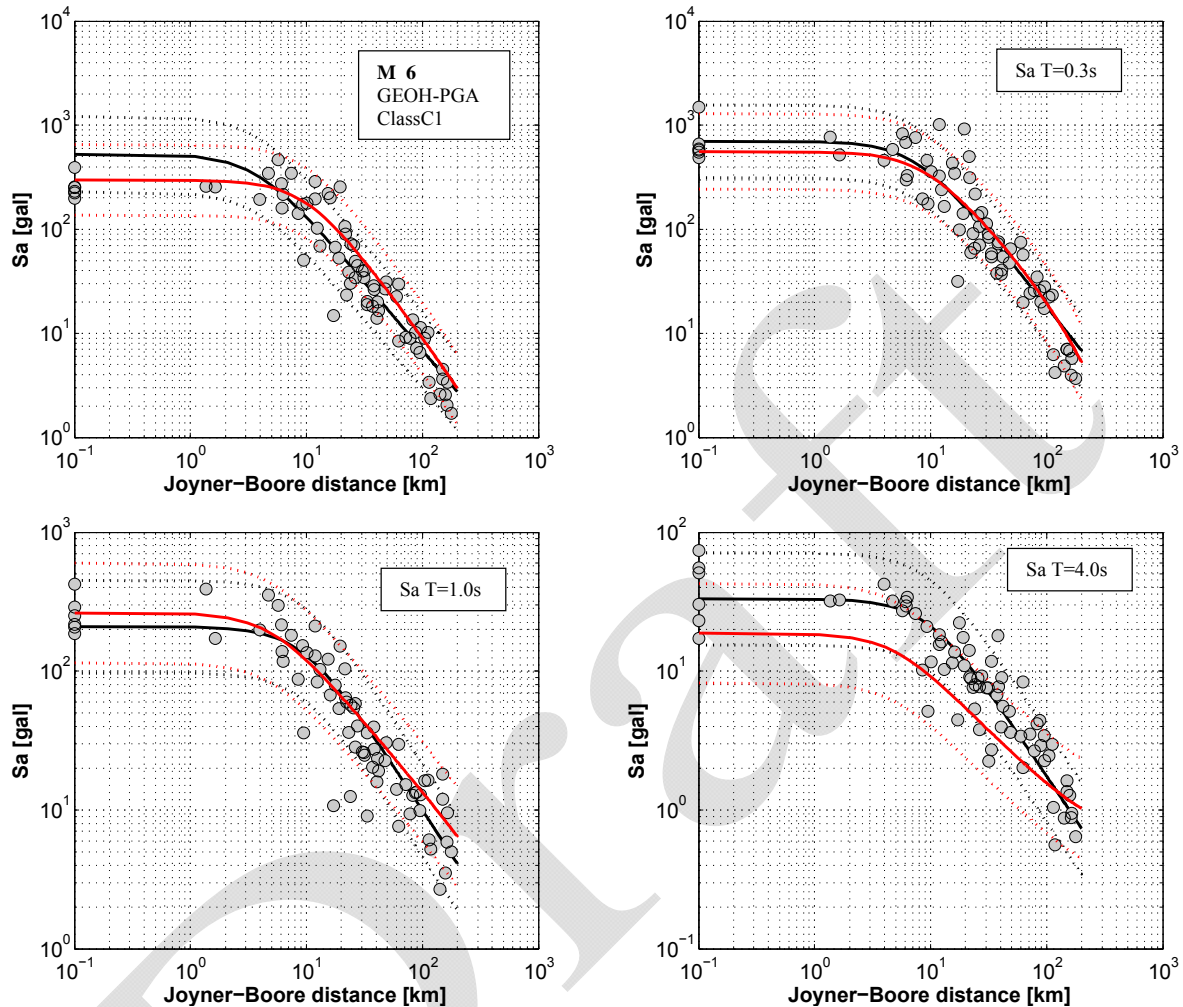


Figure 7a DBN_B-GEOH – M 6 - C1 class.

Comparisons between median predictions and 1 standard deviations (black lines for PGA and Sa at 0.3, 1.0 and 2.0s and observations (*symbols*) for thrust focal mechanism. The red lines correspond to ITA10 predictions for C class. The observations are extracted from DBN2 in the magnitude range 6.0 +/- 0.1.

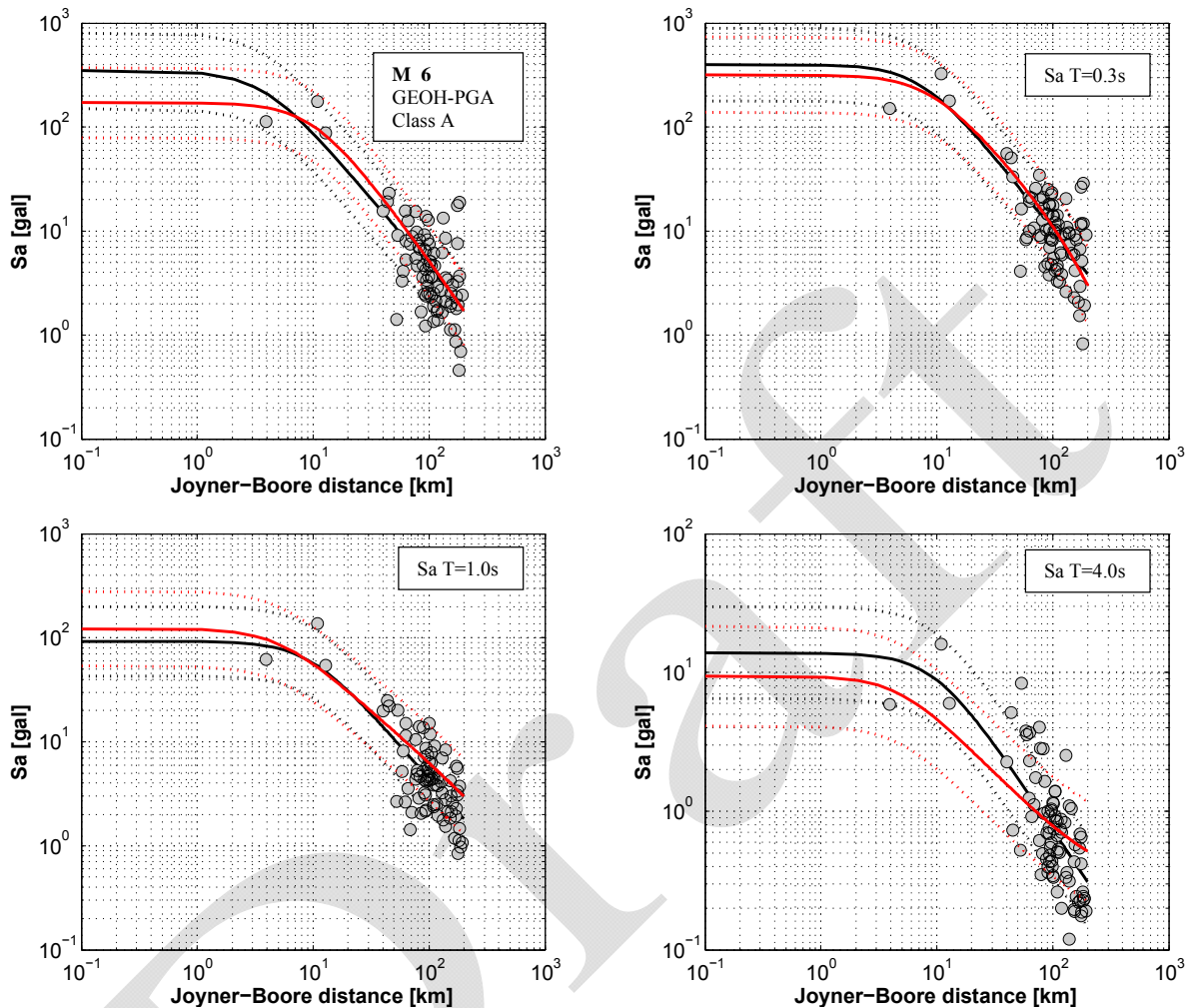


Figure 7b DBN_B-GEOH – M 6 – A class.

Comparisons between median predictions and 1 standard deviations (black lines for PGA and Sa at 0.3, 1.0 and 2.0s and observations (*symbols*) for thrust focal mechanism. The red lines correspond to ITA10 predictions for A class. The observations are extracted from DBN2 in the magnitude range 6.0 +/- 0.1.

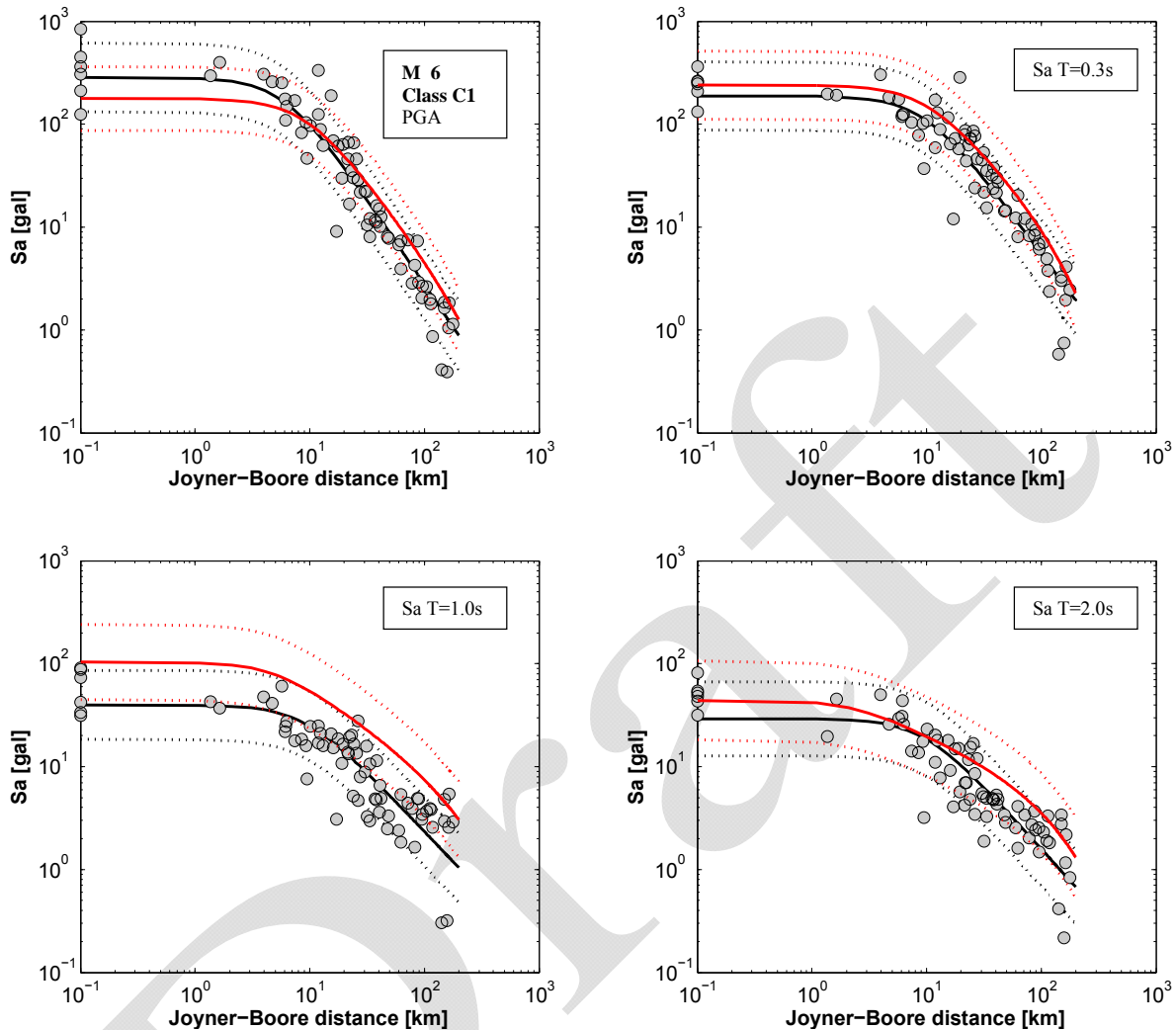


Figure 8a DBN_B-Vertical component Z – M 6 - C1 class.

Comparisons between median predictions and 1 standard deviations (black lines for PGA and S_a at 0.3, 1.0 and 2.0s and observations (*symbols*) for thrust focal mechanism. The red lines correspond to ITA10 predictions for C class. The observations are extracted from DBN2 in the magnitude range 6.0 +/- 0.1.

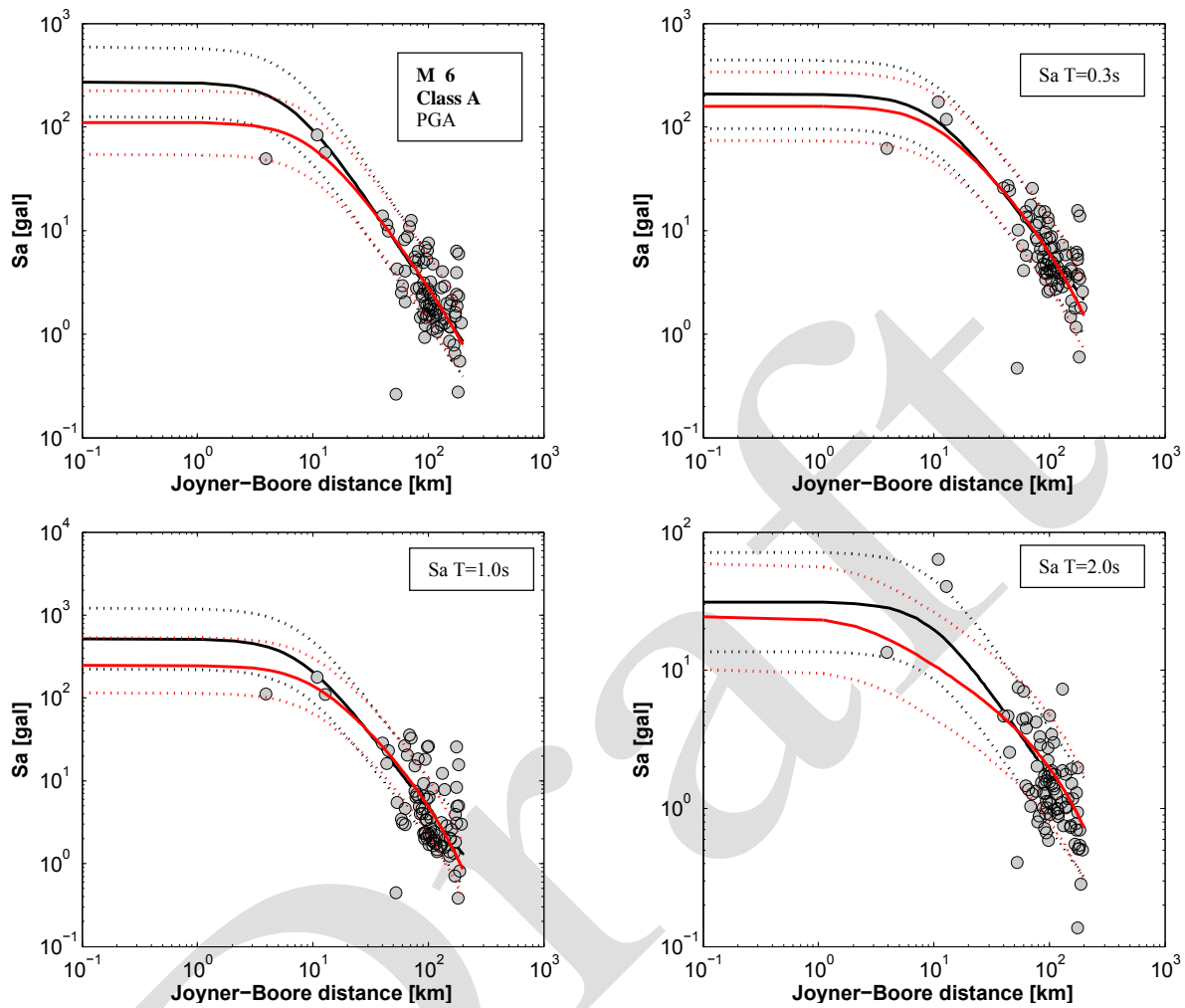


Figure 8b DBN_B-Vertical component Z – M 6 – A class.

Comparisons between median predictions and 1 standard deviations (black lines for PGA and Sa at 0.3, 1.0 and 2.0s and observations (*symbols*) for thrust focal mechanism. The red lines correspond to ITA10 predictions for class A. The observations are extracted from DBN2 in the magnitude range 6.0 +/- 0.1.

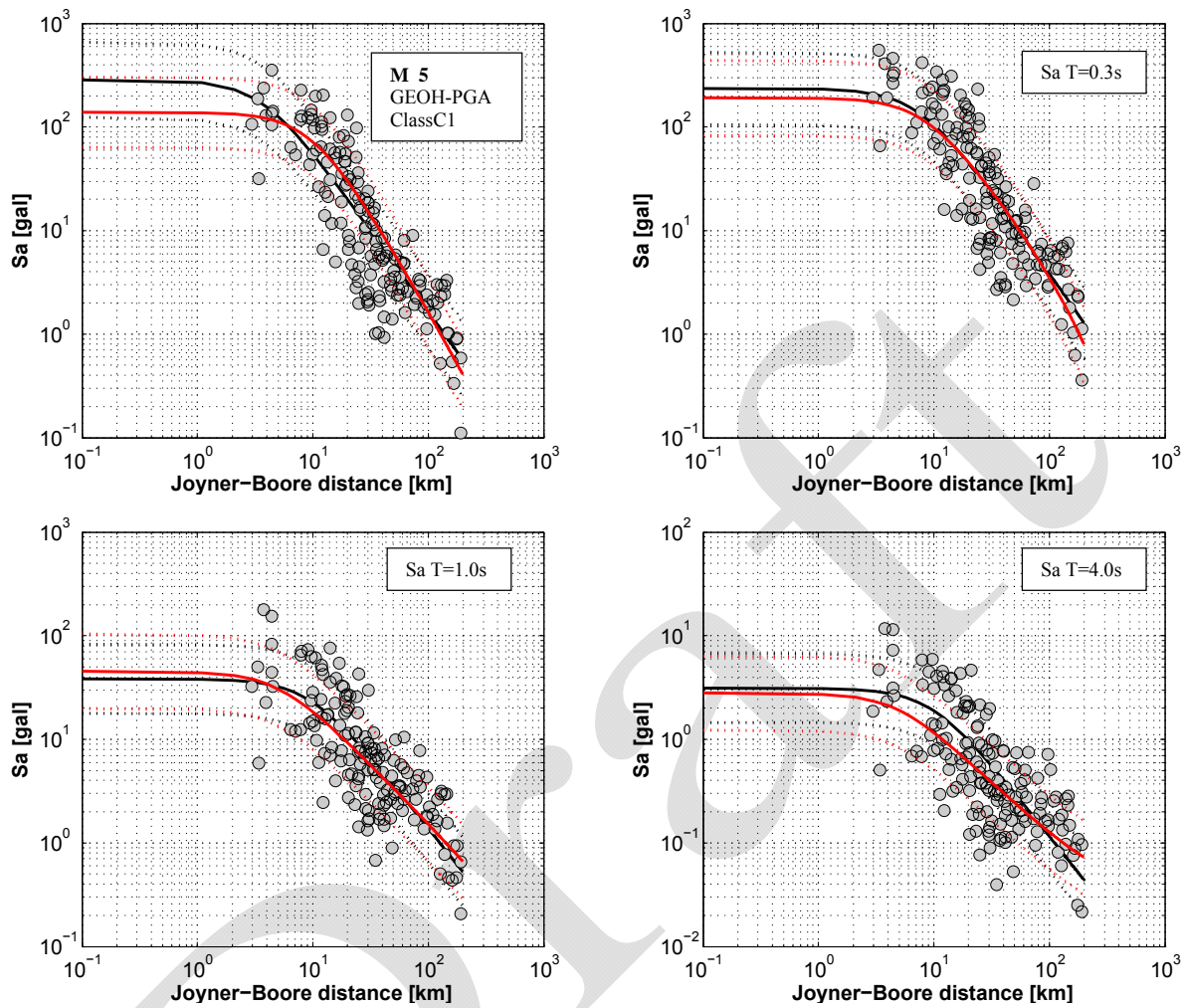


Figure 9a DBN_B-GEOH – M 5 – C1 class.

Comparisons between median predictions and 1 standard deviations (black lines for PGA and Sa at 0.3, 1.0 and 2.0s and observations (*symbols*) for thrust focal mechanism. The red lines correspond to ITA10 predictions for C class. The observations are extracted from DBN2 in the magnitude range 5.0 +/- 0.1.

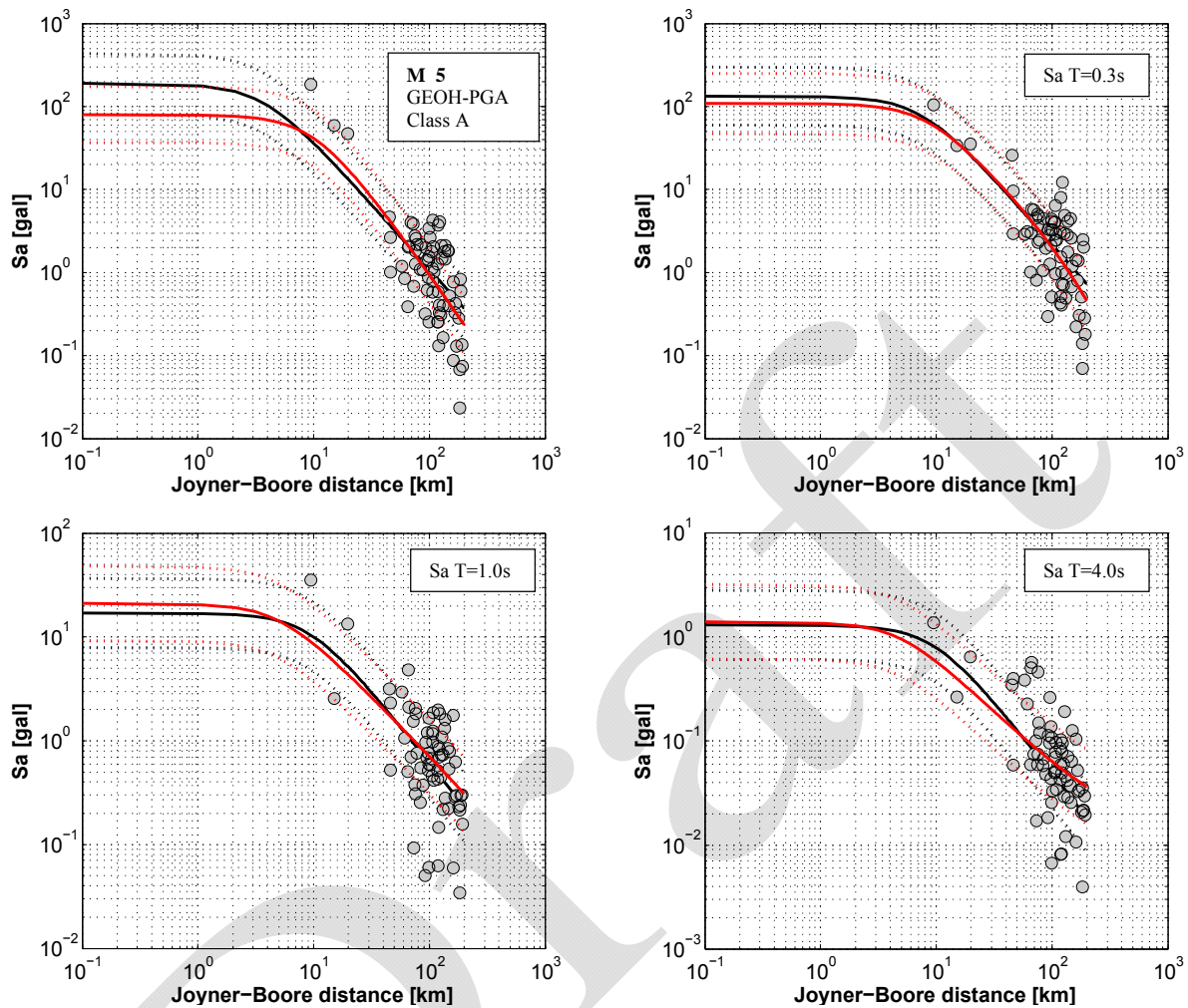


Figure 9b DBN_B-GEOH – M 5 – A class.

Comparisons between median predictions and 1 standard deviations (black lines for PGA and S_a at 0.3, 1.0 and 2.0s and observations (*symbols*) for thrust focal mechanism. The red lines correspond to ITA10 predictions for class A. The observations are extracted from DBN2 in the magnitude range 5.0 +/- 0.1.

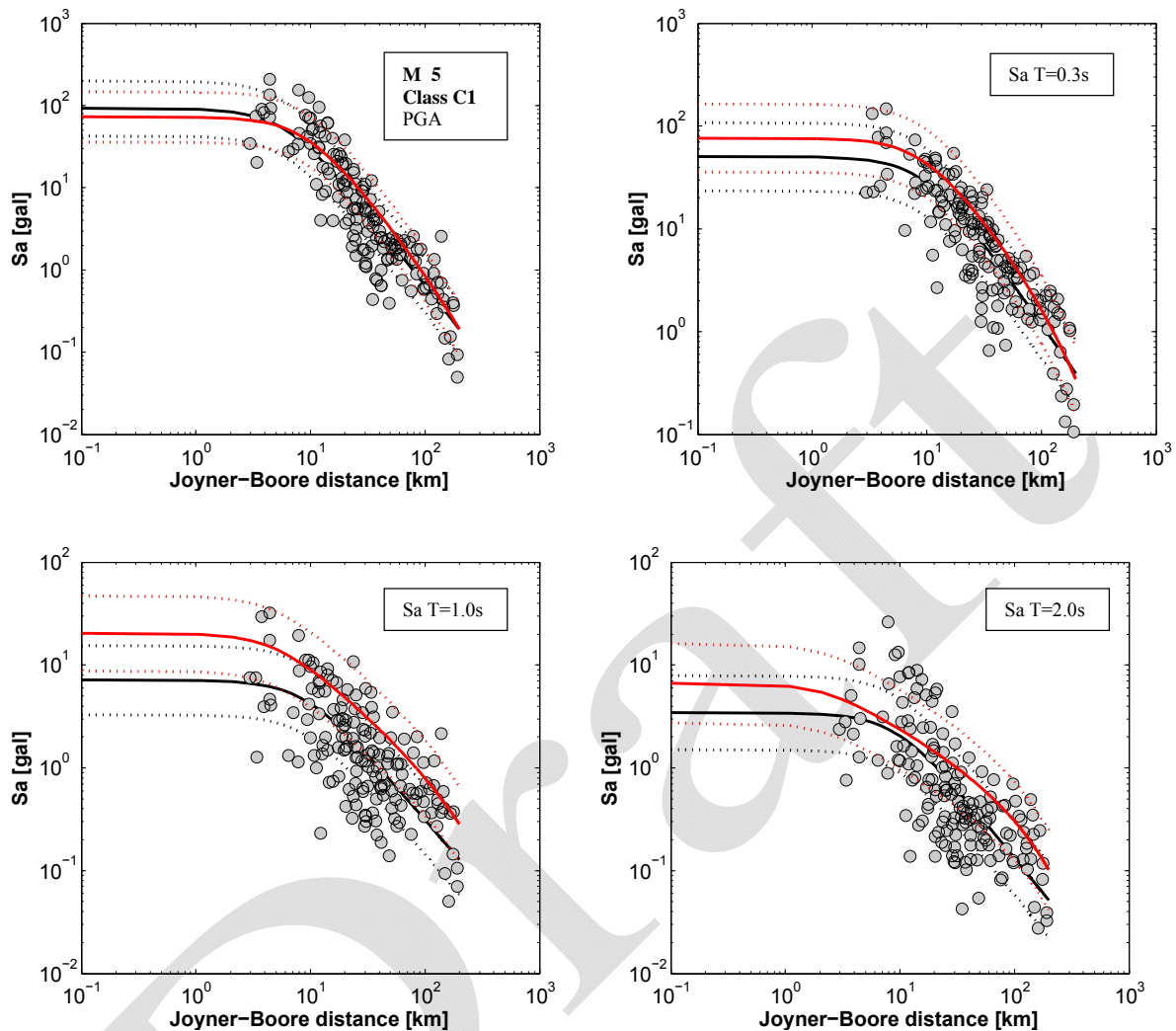


Figure 10a DBN_B-Vertical component Z – M 5 - C1 class.

Comparisons between median predictions and 1 standard deviations (black lines for PGA and Sa at 0.3, 1.0 and 2.0s and observations (*symbols*) for thrust focal mechanism. The red lines correspond to ITA10 predictions for class C1. The observations are extracted from DBN2 in the magnitude range 5.0 +/- 0.1.

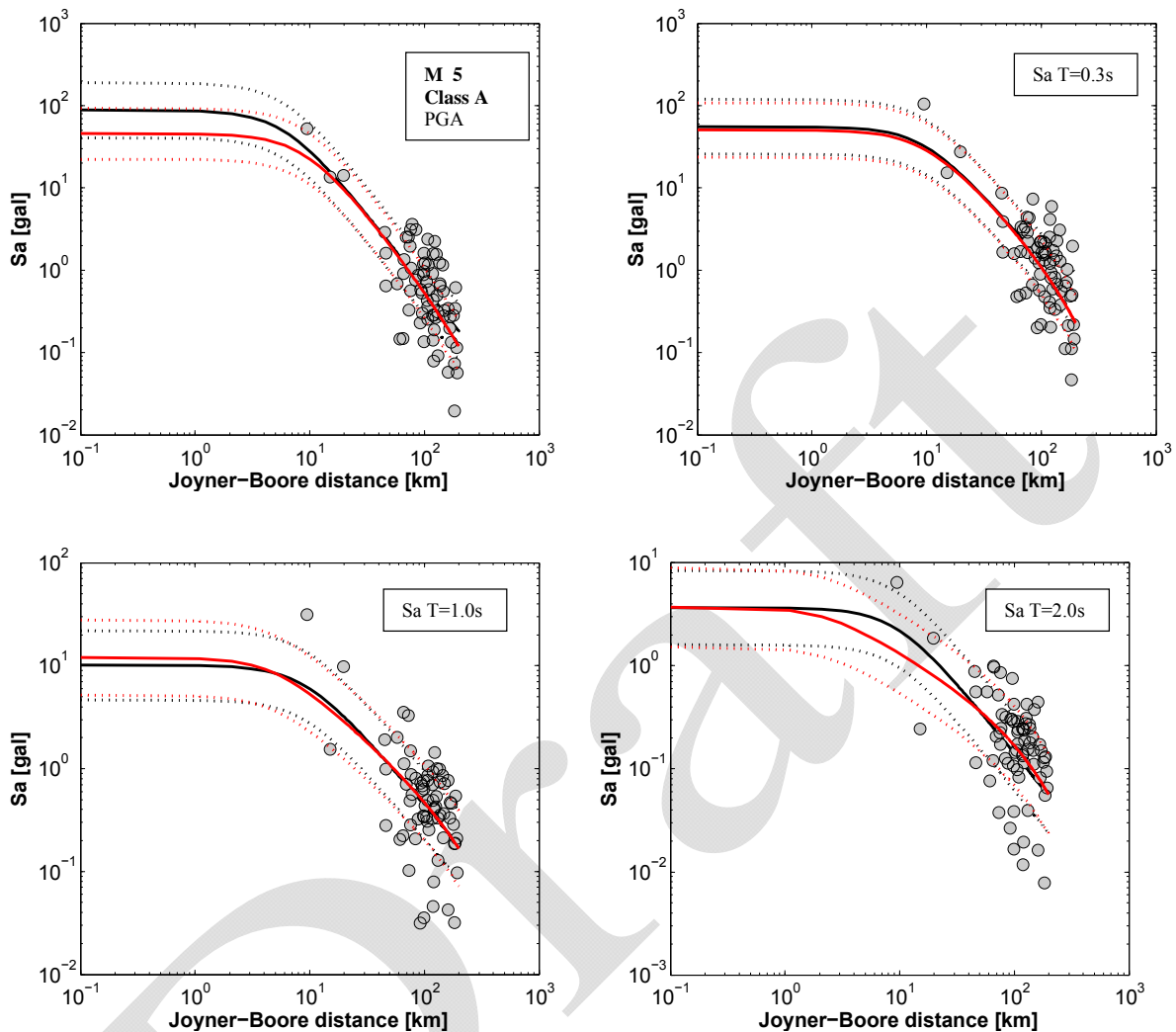



Figure 10b DBN2_B-Vertical component Z – M 5 – A class.

Comparisons between median predictions and 1 standard deviations (black lines for PGA and Sa at 0.3, 1.0 and 2.0s and observations (*symbols*) for thrust focal mechanism. The red lines correspond to ITA10 predictions for class A. The observations are extracted from DBN2 in the magnitude range 5.0 +/- 0.1.

	<p style="text-align: center;">Research and Development Programme on Seismic Ground Motion</p> <p style="text-align: center;">CONFIDENTIAL <i>Restricted to SIGMA scientific partners and members of the consortium, please do not pass around</i></p>	<p>Ref : SIGMA-2013-D2-72 Version : 01</p> <p>Date : 15 may Page : 30</p>
--	--	---

4. ANALYSIS OF RESIDUALS

4.1. Standard Deviations

Figure 11 shows the total standard deviation (σ_{tot}) as function of period, as well as the between-events and within-event components for GEOH and Z and the three considered cases.

For GEOH, the total standard deviation varies with periods from 0.32 to 0.41 (in log10 units), with the largest values at $T = 0.1s$.

For Z, the total standard deviation is almost constant with periods and varies from 0.33 to 0.37 (in log10 units).

For both components, the largest contribution comes from the within-event variability, suggesting that the high frequency variability is dominated by the between-stations term.

Among the three considered cases, the between-events variability is larger for DBN2_A and this result indicates that the use of converted magnitudes could increase the uncertainties.

Finally, the regressions performed using as explanatory variable the hypocentral distance (DBN2_BH) provide results very similar to the DBN2_B, where the Joyner and Boore distance is adopted.

Figure 11 also reports the σ_{tot} of ITA10 model. The standard deviations for the regional and Italian models are similar, with a slight reduction for periods longer than 0.4s for the regional models in case of GEOH, while the opposite occurs at short periods.

This result suggests that the introduction of the C1 class improves the long-period seismic response of sites in the Po plain, while the proposed model might not be suitable to capture the large high frequency variability of the response for the rock and stiff sites.

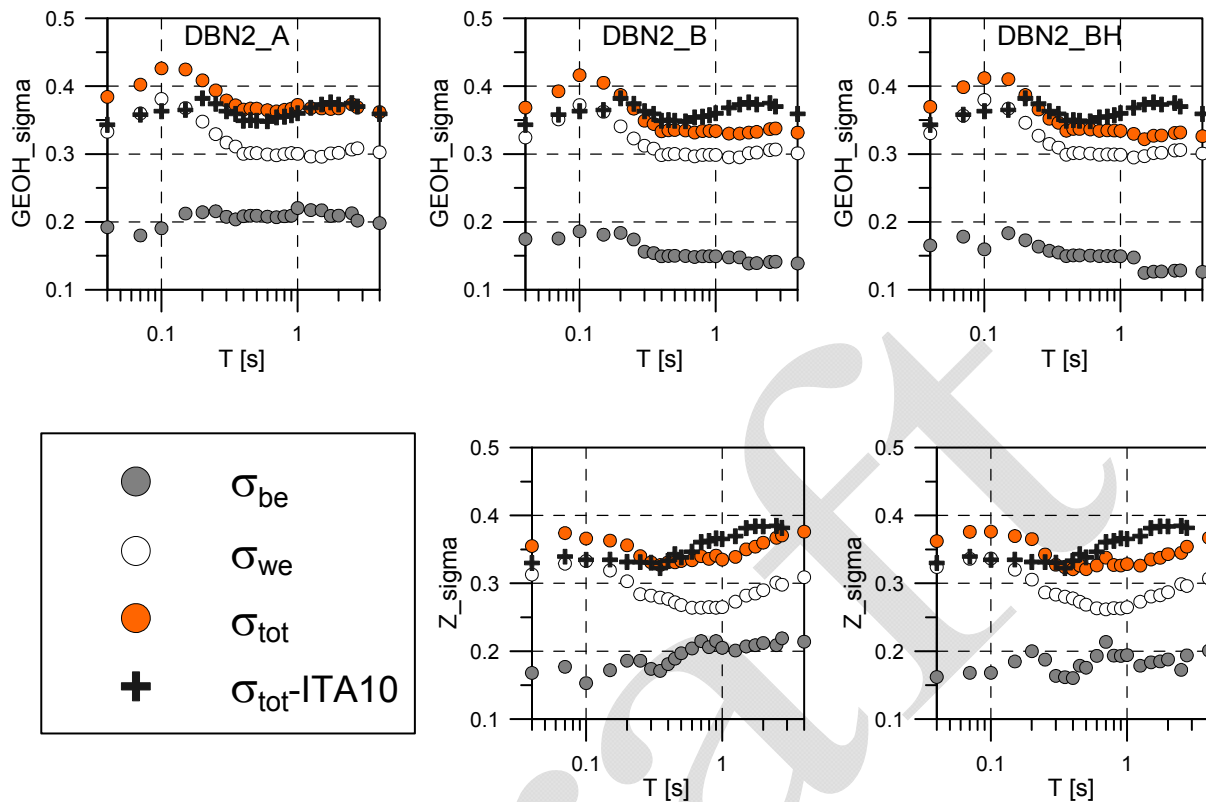


Figure 11. Period-dependent total standard deviation (σ_{tot}) of the GMPE derived in this study (orange circles) or GEOH (Top) and Z (Bottom). The total standard deviation for ITA10 is also reported.


4.1. Decomposition of the residuals

In this section, we decompose the total residuals into different parts (Scasserra et al., 2009; Al Atik et al., 2011) with the aim of investigating the possible causes of uncertainties that are not captured by the models calibrated in this study. The residual analysis is carried out using DBN2_B dataset and associated ground motion prediction equations.

This is accomplished by decomposing the residuals according to the following expression:

$$R_{ij} = \delta B_i + \delta W_{ij} \quad [4]$$

where the subscripts i and j refer to *event* and *station*, respectively.

	Research and Development Programme on Seismic Ground Motion CONFIDENTIAL <i>Restricted to SIGMA scientific partners and members of the consortium, please do not pass around</i>	Ref : SIGMA-2013-D2-72 Version : 01 Date : 15 may Page : 32
--	--	--

R_{ij} is computed as the difference between the logarithm (base 10) of observation and prediction, δB_t represents is the between-events residual, which corresponds to the average misfit of recordings of one particular earthquake with respect to the median ground-motion model, and δW_{ij} represents the within-event residual, which corresponds to the difference between the total residual and δB_t .

Following the approach of Rodriguez-Marek (2011), the within-event residuals are then exploited to evaluate the site term for each station j :

$$\delta S2S_j = \frac{1}{NE_j} \sum_{t=1}^{NE_j} \delta W_{ij} \quad [5]$$

Where NE_j is the number of events recorded at station j .

This term quantifies the average misfit of recordings from one particular site with respect to the event-corrected median ground-motion.

The within-event residual can be written as:

$$\delta W_{ij} = \delta S2S_j + \delta W_{o,ij} \quad [6]$$

where $\delta W_{o,ij}$ is the remaining residual after site and events terms are subtracted from total residuals.

Distance scaling

Distance scaling is tested by examining trends of total residuals R_{ij} , the within-event residuals δW_{ij} and the event and site corrected residuals $\delta W_{o,ij}$ as a function of distance.

Figures 12 shows the distribution of the total residuals and within-event residuals at different periods (0.1s and 2.0s). The R_{ij} and δW_{ij} distributions have similar trends, indicating that the corrections for the event term is irrelevant for distance scaling. Both residuals are in the range -1./+1.

For both residuals a complex trend with distance is observed at short periods: the residuals present two bumps centered around 10 and 100km, respectively, while negative values are observed in the

range 30 – 60 km (i.e. observations lower than predictions). Conversely, at longer periods the residuals show a weaker dependence on distance.

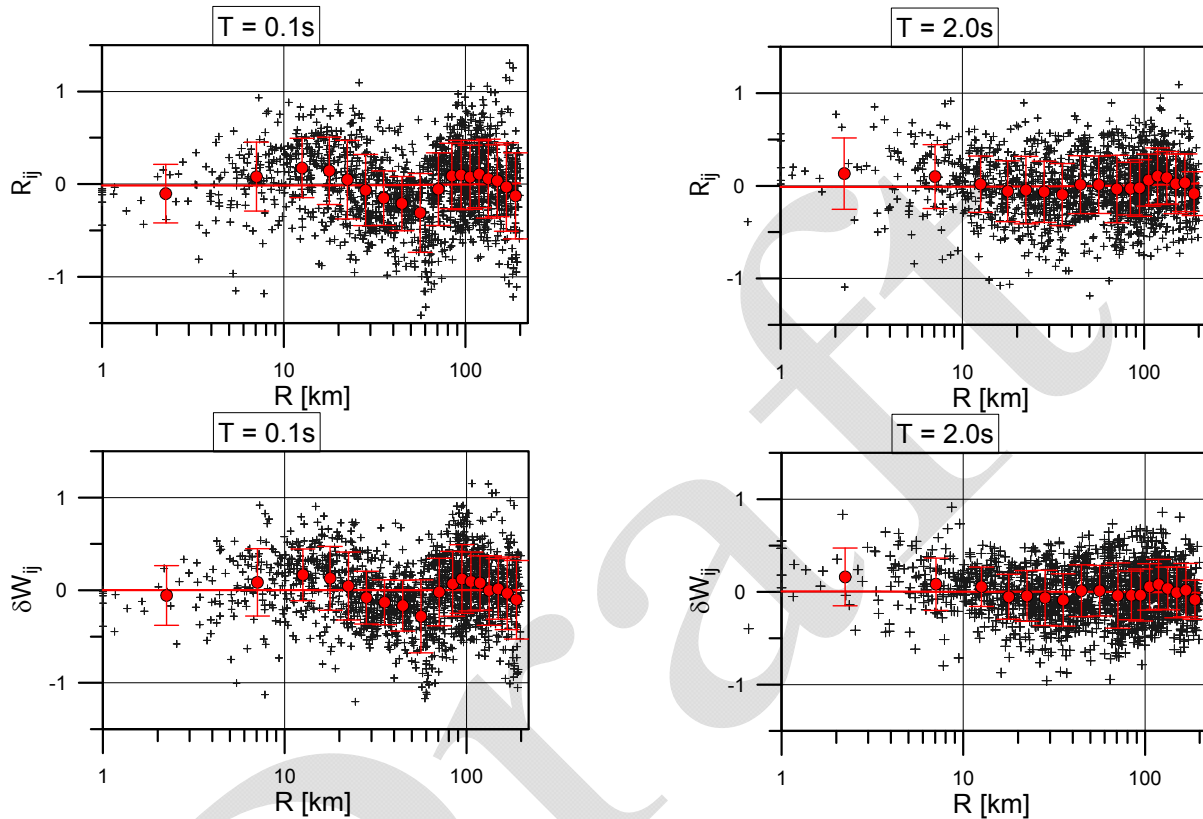


Figure 12. Total residuals (top), computed as $\log_{10}(\text{observation}/\text{prediction})$ and within-event residuals (bottom) for GEOH at selected periods as a function of distance.

In Figure 13 we plot the distribution of the residuals corrected for the event and site terms ($\delta W_{o,tj}$). In this case, no dependence on distance and frequency is observed and the residuals are within $-0.5/+0.5$ with very few exceptions.

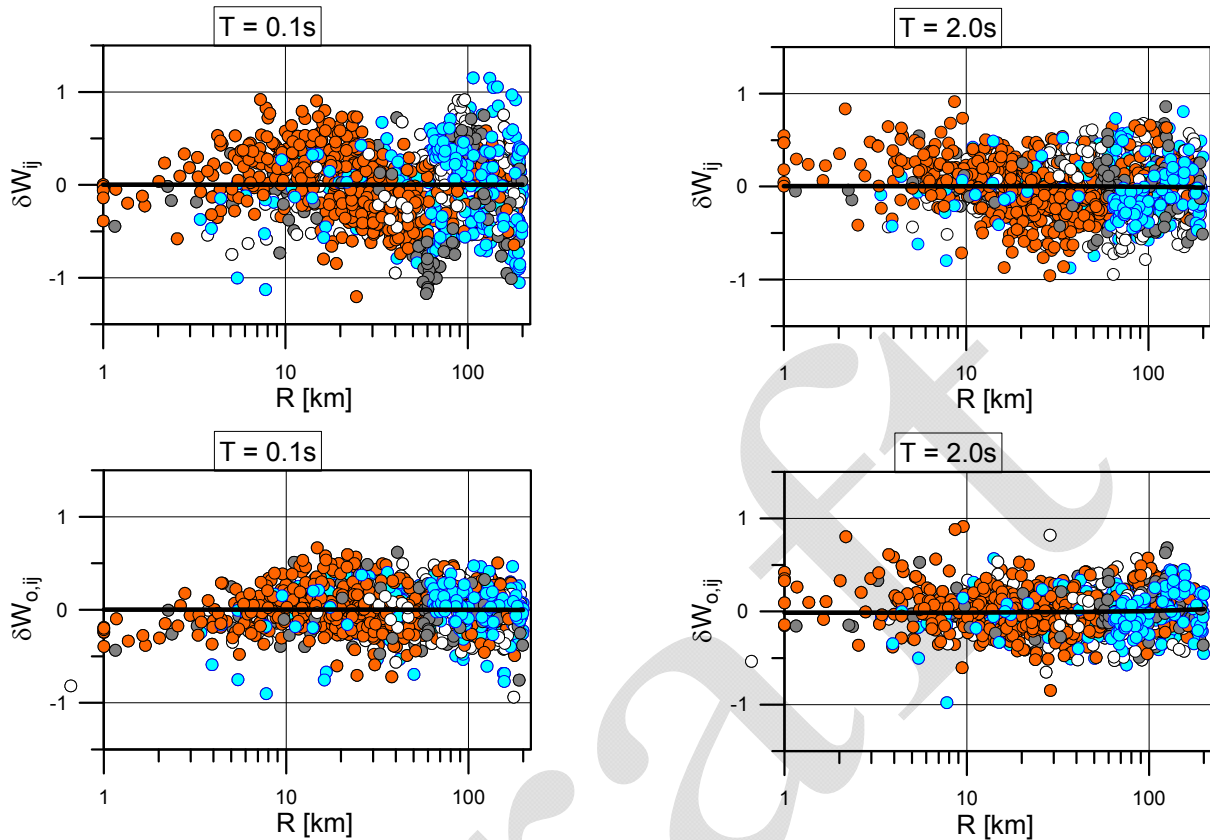


Figure 13. Within-events residuals (top) and site-event corrected residuals (bottom) for GEOH spectral ordinates at selected periods as a function of distance. The residuals are grouped according to the EC8 site classification (classes A: blue; classes B: grey; class C: white; class C1: orange)

We have to recall that most of the recordings are relative to the Emilia seismic sequence and the obtained results could indicate that site and propagation effects occur at recurring distance ranges, and that the contribution due to source, propagation and site cannot be simply separated. For the same reason the BDN2_B dataset is characterized by site classes that are not uniformly distributed over distance, since C and C1 sites are mainly located in epicentral area and A and B sites are far from the seismic sources. In this way, at larger distance, high-frequency amplification and low frequency de-amplification for rock and stiff sites may bias the attenuation term. Similarly, at shorter distance, propagation effects through the Po plain and source effects may affect the ground motion, thus influencing the distance scaling.

Magnitude scaling

Magnitude scaling is tested examining the between-events error as a function of the magnitude.

Figure 14 shows the distribution of the between-events errors for the 78 earthquakes of the DBN2_B dataset, plotted at different periods. Although the variation is within ± 0.5 , we observe that the largest error occurs for events with magnitude less than 5 and in the correspondence of the events of the past (in particular the Friuli 1976 sequence).

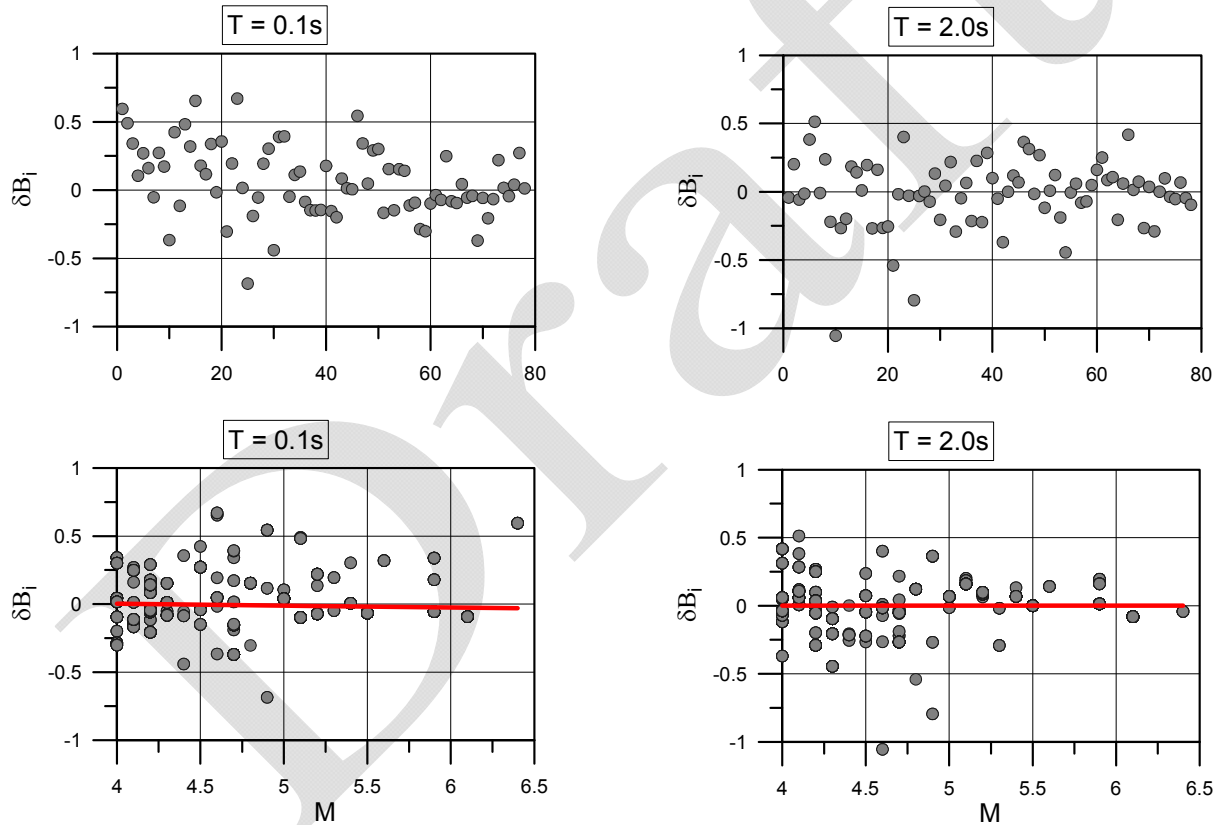


Figure 14. Between-events errors as a function of id events (chronologically ordered) and magnitude for 78 earthquakes of the DBN2_B dataset.

Site scaling

The site scaling is tested by examining distributions of between-stations residuals, δS_j .

Figure 15 shows the between-stations residuals for horizontal components for two periods, 0.1s and 2s, considering the data set grouped according to the classification scheme used in this study.

A large dispersion of the between-stations residuals is observed, mainly for class A and B in the short to medium period range. At longer periods, the dispersion diminishes. In the case of classes C and C1, most of site terms are in the range ± 0.5 .

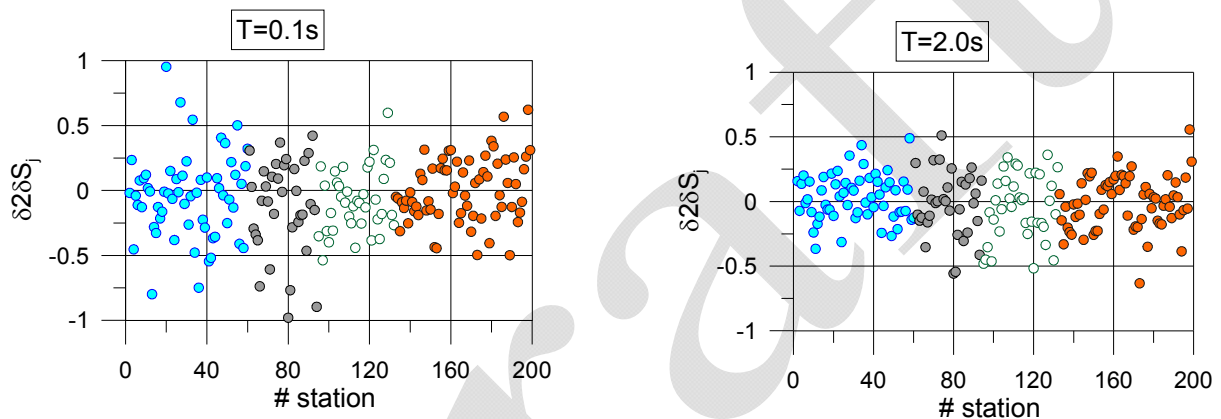


Figure 15. Between-stations errors. The circles have colors which indicate the EC8 classes (colors from blue to orange correspond to classes A through C1, respectively).

In the following, we illustrate (Figure 16 and 17) some examples of the between-stations error distributions for specific sites that are well sampled, having more than 5 records.

Figure 16 shows the residuals for some sites belonging to classes A and B.

Stations MLC, ZEN8 (class A*) and VOBA (Class B*) have the peak amplifications in correspondence of short periods, that cannot be captured by a flat or broad band response site, as indicated by the coefficients of the GMPE. On the other hand, other stations, as MTRZ (A* class), are amplified at long periods, indicating that either they were badly classified or the surface wave travelling in the plain could affect the ground motion of sites located at the border of the Po plain.

Figure 17 shows the residuals for some sites belonging to classes C and C1.

In general for these stations, low-frequency amplification is adequately described by the site coefficients of the GMPE.

On the other hand, sites located very close to the earthquakes epicentres, show extremely variable site effects: (MRN, class C1) is amplified with respect to the average response of C1 sites, CAS03, T0821 (class C1) are de-amplified at all periods and other sites (T0813 and T0826, class C1) present a specific peak at high-frequency, indicating that source effects may strongly affect the response at these stations, as well as the interaction with subsurface geology.

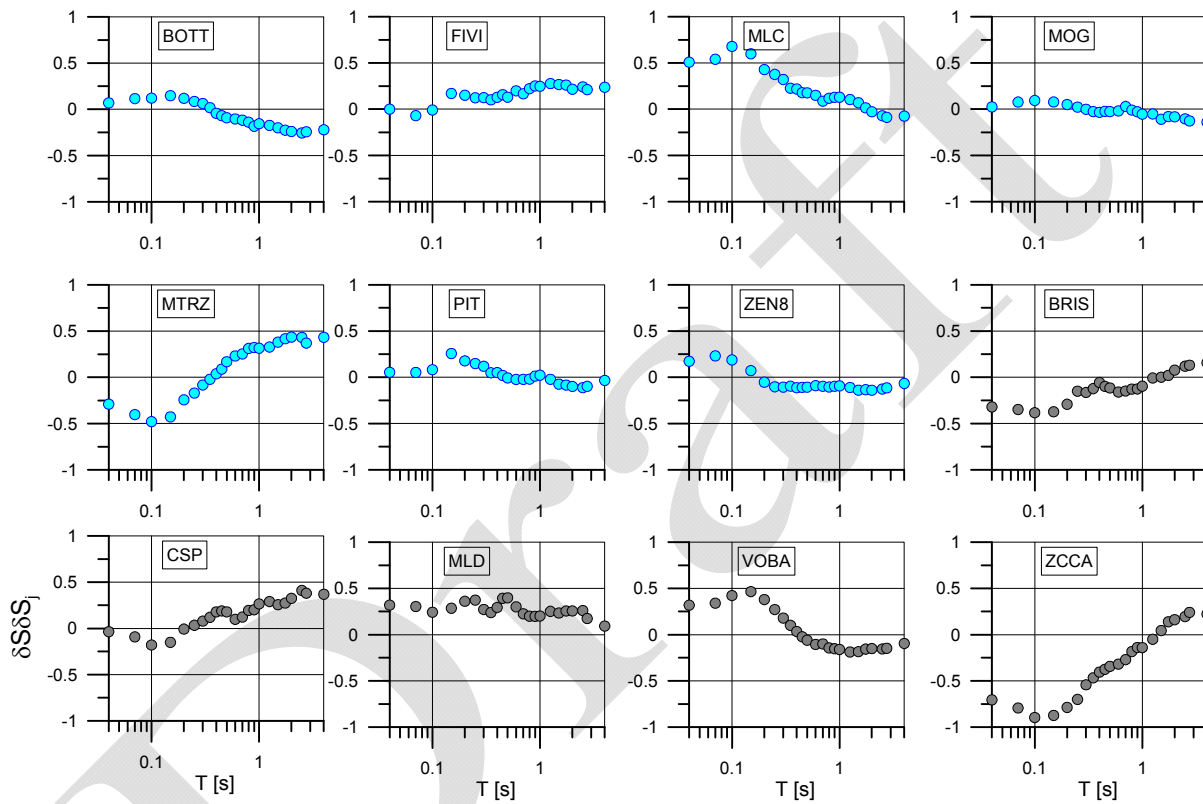


Figure 16.- Period dependence of the between-station residuals for a set of stations belonging to A and B classes

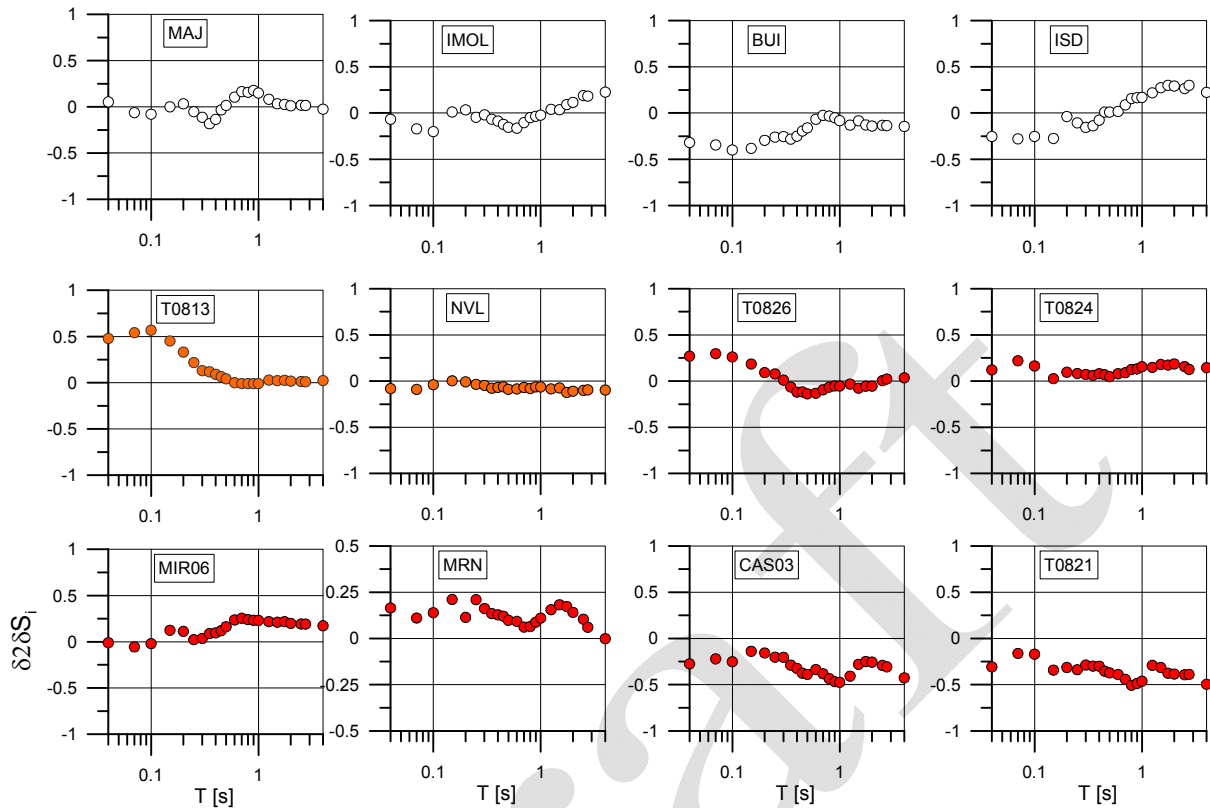


Figure 17 - Period dependence of the between-station residuals for a set of stations belonging to C and C1 classes.

Single station sigma

Figure 18 displays, for the sites T0821 (Casaglia, class C1) and NVL (Novellara, class C1), selected within the Sigma project as the test-sites for hazard studies, the site terms in the period range 0.04 – 4s, together with the event-corrected single-station sigma for each site $\phi_{ss,s}$, defined as (Rodriguez-Marek et al: 2011):

$$\phi_{ss,s} = \sqrt{\frac{\sum_{i=1}^{NE_j} (\delta W_{ij} - \delta S_j)^2}{NE_j - 1}} \quad [4]$$

For the sake of comparison, we also reported the results for MRN and MIR06 stations (class C1), located very close and at about 20-30 km from the sources of the 2012 Emilia seismic sequences, respectively.

Site terms close to zero mean that the station, on average, has a response that follows closely its class. Positive site terms mean that, on average, the residuals of the station, corrected for the between-events error, indicate amplification with respect to its class, while negative terms mean de-amplification.

NVL, that recorded several events of the 2012 Emilia seismic sequence as well events of the past (i.e. Parma 1996), has a negligible site term, close to zero, indicating a similar response to the average response of the class; however its variability is very high especially at long periods, showing that the site response could vary depending on the seismic sources and source to site paths. T0821, a temporary station installed after the 20 May 2012 earthquake at about 20-30 km from the epicentral area, show de-amplification with respect to its class, for the entire period range, but low variability (sigma equals to about 0.15 units), indicating a stable behaviour, probably because of seismic sources and source to site paths are very similar.

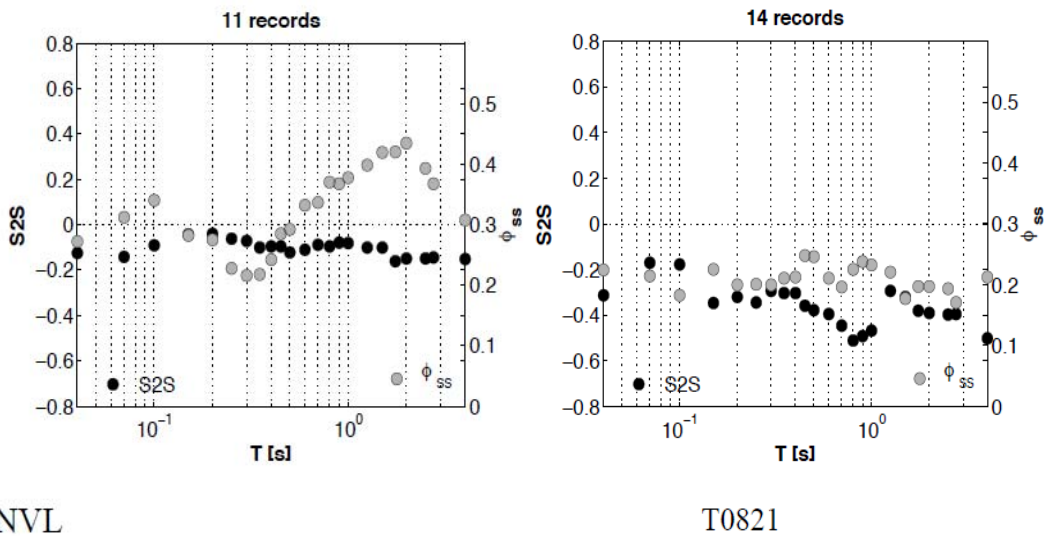


Figure 18. Site error (black dots) and single station sigma (grey dots) for NVL and T0821 sites. Left y-axis is relative to the site term; right y-axis is relative to the single station sigma.

Finally, as illustrated in Figure 19, the response of station MRN is amplified in the entire period range with a single station sigma varying from 0.2 to 0.3, while MIR06 is amplified only at long

periods, but associated to a smaller standard deviation (around 0.15 units). This could indicate that, in near source, the details of the rupture affect the site response.

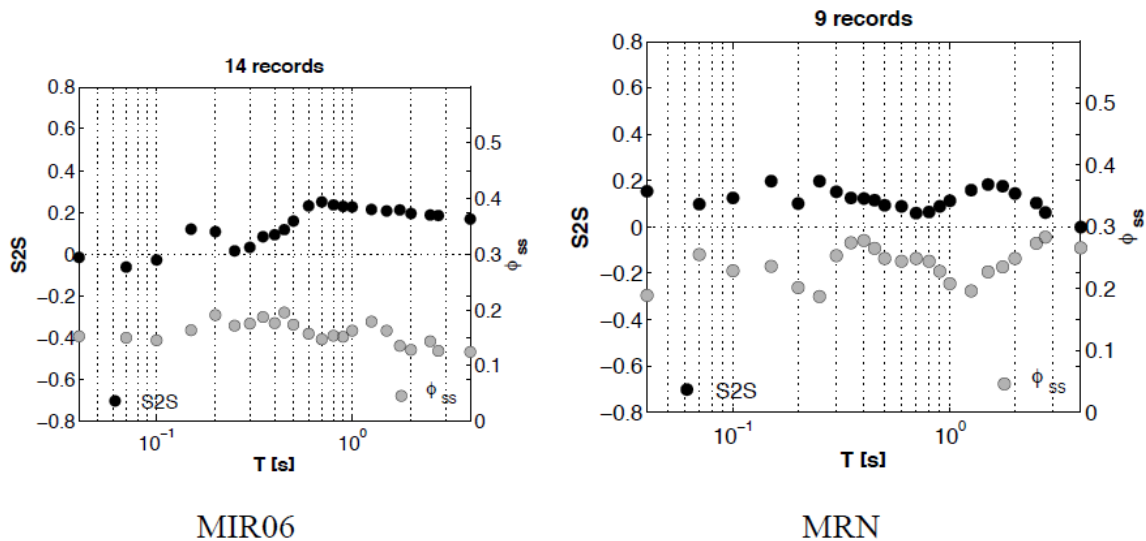



Figure 19. Site error (black dots) and single station sigma (grey dots) for NVL and T0821 sites. Left y-axis is relative to the site term; right y-axis is relative to the single station sigma.

5. CONCLUSIONS

In this work, we updated the DBN strong motion dataset for northern Italy, realized within the SIGMA project and delivered in November 2012 (deliverable SIGMA-2012-D2-53_02), adding new records and improving the station and event metadata. The new dataset, called DBN2, is composed by 2174 waveforms, recorded in the period 1976 (Friuli sequence) – 2012 (Emilia sequence). It includes 136 earthquakes (109 of them recorded by more than 1 stations) and 299 stations (248 of them having more than 1 records). The Emilia sequence provides about the 2/3 of the entire dataset of northern Italy.

We exploited DBN2 to extract a qualified dataset to develop a set of GMPEs for northern Italy.

The regressions have been performed for PGA and spectral acceleration, considering the geometrical mean of the NS and EW components and the vertical component, in the magnitude range 4–6.4, for distances up to 200 km and hypocentral depth within 30 km.

	<p>Research and Development Programme on Seismic Ground Motion</p> <p>CONFIDENTIAL <i>Restricted to SIGMA scientific partners and members of the consortium, please do not pass around</i></p>	<p>Ref : SIGMA-2013-D2-72 Version : 01</p> <p>Date : 15 may Page : 41</p>
--	--	---

The model is adequately calibrated, as the observations have no significant bias affecting the between-events or the within-event distribution of errors. The total standard deviation (σ_{tot}) varies between 0.32 and 0.41 log₁₀ unit, with the largest values observed at short periods.

This set of new GMPEs improves the existing attenuation equation derived for northern Italy, however it should be used with some recommendations, since the compiled North Italy data set is characterized by an unbalanced number of recordings (majority of thrust or reverse style of faulting, class A and B sites at large distance and C1 sites at short distances).


As a consequence, the GMPEs derived in this study are proposed to evaluate the PGA and spectral ordinates in the Po plain area especially for C1 sites and thrust faults. For the rest of the cases (other styles of faulting and soil categories) the use of the GMPEs derived by Bindi et al (2011) for the Italian territory is recommended.

We tested two different datasets (DBN2_A and DB2_B): in the former the local magnitude M_l is converted in M_w using the equation by Castello et al. (2007), while, in the latter, both M_l and M_w are considered. We found that the conversion between M_l and M_w leads to a larger standard deviation and, in particular, it affects the between-events component of variability. This result suggests that, for an optimal use of the GMPE, the M_w should be used only when available, otherwise the use of M_l is recommended.

The main outcomes of the residual analysis are:

- 1) the events of the past (pre1990's) are characterized by large between-events errors, maybe due to the uncertain location and magnitude estimation of the events;
- 2) the largest part of the variability is carried by the within-event component, probably attributable to the large variation of the response at the sites, that cannot be separated by the propagation and source effects in several cases (Figure 12). An additional cause of variability might be attributed to the reflection of the body waves from the Moho contained in many recordings, as observed by various authors (Bragato et al., 2011);
- 3) the between-stations error is extremely variable even for C1 sites which are expected to have very similar geological features;
- 4) the single-station sigma is generally high at short distances from the seismic source, as observed in the case of MRN.

Finally, it is worth to note that in this study, nonlinear or 2D and 3D effects, due to the propagation of surface waves, have not been considered, as they need additional analysis.

	<p>Research and Development Programme on Seismic Ground Motion</p> <p>CONFIDENTIAL</p> <p><i>Restricted to SIGMA scientific partners and members of the consortium, please do not pass around</i></p>	<p>Ref : SIGMA-2013-D2-72 Version : 01</p> <p>Date : 15 may Page : 42</p>
--	---	---

6. REFERENCE

Abrahamson, N. A., and R. R. Youngs (1992), A stable algorithm for regression Analyses using The Random Effects Model, *Bull. Seismol. Soc. Am.*, 82(1), 505–510

Atik, L., N. A. Abrahamson, J. J. Bommer, F. Scherbaum, F. Cotton, and N. Kuehn (2010), The Variability of Ground-Motion Prediction Models and Its Components, *Seismol. Res. Lett.*, 81(5), 794–801, doi:10.1785/gssrl.81.5.794

Bindi D., Pacor F., Luzi, Puglia R., Massa M., Ameri G., Paolucci R., (2011). Ground motion prediction equations derived from the Italian strong motion database. *Bulletin of earthquake engineering*, vol. 9, p. 1899-1620.

Bordoni P., Azzara R., Cara F., Cogliano R., Cultrera G., Di Giulio G., Fodarella A., Milana G., Pupillo S., Riccio G., Rovelli A., Augliera P., Luzi L., Lovati S., Massa M., Pacor F., Puglia R., Ameri G., (2012). Site effects in epicentral area of the 2012 Emilia seismic sequence from EMERSITO, the rapid response network for seismic effect studies. *Annals of Geophysics*, vol. 55, 4, pp. 599-607, doi: 10.4401/ag-6153.

Bragato, P. L., Sukan, M. Augliera, P. Massa, M., Vuan, A. and A. Sarao (2011). Moho Reflection Effects in the Po Plain (Northern Italy) Observed from Instrumental and Intensity Data. *Bulletin of the Seismological Society of America*, Vol. 101, 2142–2152.

Carta Geomorfologica della Pianura Padana. Stralcio Carta Geomorfologica della Pianura Padana edita dal Ministero dell'Università e della Ricerca scientifica e tecnologica – Comitato Consultivo del C.N.U. n°4 “Scienze della Terra” – 1997. Scala 1: 250.000).


Castello B., Selvaggi G., Chiarabba C., Amato A., 2006. CSI Catalogo della sismicità italiana 1981-2002, versione 1.1. INGV-CNT, Roma <http://csi.rm.ingv.it/>

Castello B., Olivieri M., Selvaggi G- (2007). Local and Duration Magnitude Determination for the Italian Earthquake Catalog, 1981–2002, *Bulletin of the Seismological Society of America*, Vol. 97, 128–139.

Comité Européen de Normalisation (CEN) (2004). Eurocode 8: Design of Structures for Earthquake Resistance—Part 1: General Rules, Seismic Actions and Rules for Buildings. Brussels: Comité Européen de Normalisation.

De Natale G. D., Madariaga R., Scarpa R. and A. Zollo (1987). Source Parameter Analysis from Strong Motion Records of the Friuli, Italy, Earthquake Sequence (1976-1977). *Bulletin of the Seismological Society of America*, Vol. 77, 1127–1987.

Di Capua, G., G. Lanzo, V. Pessina, S. Peppoloni, and G. Scasserra (2011). The recording stations of the Italian strong motion network: geological information and site classification, *Bulletin of Earthquake Engineering*, 9, 1779-1796, doi:10.1007/s10518-011-9326-7.

	<p style="text-align: center;">Research and Development Programme on Seismic Ground Motion</p> <p style="text-align: center;">CONFIDENTIAL <i>Restricted to SIGMA scientific partners and members of the consortium, please do not pass around</i></p>	<p>Ref : SIGMA-2013-D2-72 Version : 01</p> <hr/> <p>Date : 15 may Page : 43</p>
--	--	---

DISS Working Group (2010), Database of Individual Seismogenic Sources (DISS), Version 3.1.01: A compilation of potential sources for earthquakes larger than M 5.5 in Italy and surrounding areas, <http://diss.rm.ingv.it/diss/>.

Hanks, T. C. (1975). Strong ground motion of the San Fernando, California, earthquake: ground displacements, *Bulletin of the Seismological Society of America*, 65, 193–225.

Hisada Y., Aki K., Teng T. (1993). Application of Non stationary Ray Decomposition to Identifying Deep Seismic Bedrock of the Kanto Sedimentary Basin, Japan. *Bulletin of the Seismological Society of America*, Vol. 83, 1700-1720

ISIDe Working Group (INGV, 2010), Italian Seismological Instrumental and parametric database: <http://iside.rm.ingv.it>.

ITACA Working Group (2010). Data Base of the Italian strong motion records: <http://itaca.mi.ingv.it>

Joyner W. B. (2000). Strong Motion from Surface Waves in Deep Sedimentary Basin. *Bulletin of the Seismological Society of America*, vol. 90, S95-S112.


Kagawa, T., B. Zhao, K. Miyakoshi, and K. Irikura (2004). Modeling of 3D Basin Structures for Seismic Wave Simulations Based on Available Information on the Target Area: Case Study of the Osaka Basin, Japan. *Bulletin of the Seismological Society of America*, Vol. 94, 1353-1368.

Luzi L., Pacor F., Ameri G., Puglia R., Burrato P., Massa M., Augliera P., Franceschina G., Lovati S. and R. Castro (2013). Overview on the strong motion data recorded during the May-June 2012 Emilia seismic sequence, accepted to *Seismological Research Letter*

Moretti M., Abruzzese L., Abu Zeid N., Augliera P., Azzara R., Barnaba C., Benedetti L., Bono A., Bordoni P., Boxberger T., Bucci A., Cacciaguerra S., Calò M., Cara F., Carannante S., Cardinale V., Castagnozzi A., Cattaneo M., Cavaliere A., Cecere G., Chiarabba C., Chiaraluce L., Ciaccio M.G., Cogliano R., Colasanti G., Colasanti M., Cornou C., Courboux F., Criscuolo F., Cultrera G., D'Alema E., D'Ambrosio C., Danesi S., De Gori P., Delladio A., De Luca G., Demartin M., Di Giulio G., Dorbath C., Ercolani E., Faenza L., Falco L., Fiaschi A., Ficeli P., Fodarella A., Franceschi D., Franceschina G., Frapiccini M., Frogneux M., Giovani L., Govoni A., Improta L., Jacques E., Ladina C., Langlaude P., Lauciani V., Lolli B., Lovati S., Lucente F.P., Luzi L., Mandiello A., Marocci C., Margheriti L., Marzorati S., Massa M., Mazza S., Mercierat D., Milana G., Minichiello F., Molli G., Monachesi G., Morelli A., Moschillo R., Pacor F., Piccinini D., Piccolini U., Pignone M., Pintore S., Pondrelli S., Priolo E., Pucillo S., Quintiliani M., Riccio G., Romanelli M., Rovelli A., Salimbeni S., Sandri L., Selvaggi G., Serratore A., Silvestri M., Valoroso L., Van der Woerd J., Vannucci G., Zaccarelli L. (2012). Rapid-response to the earthquake emergency of May 2012 in the Po Plain, Northern Italy. *Annals of Geophysics*, "The Emilia (northern Italy) seismic sequence of May-June, 2012: preliminary data and results" edited by Marco Anzidei, Alessandra Maramai and Paola Montone, vol. 55, n. 4, 2012; pp. 583-590, doi: 10.4401/ag-6152.

Pacor F., Luzi L., Massa M., Bindi D. (2012). Ranking of available GMPEs from residual analysis for northern Italy and definition of reference GMPEs. SIGMA Project, Deliverable SIGMA-2012-D2-53-02.

Pacor F., Luzi L., D'Amico M., Puglia R. and Bindi D. (2013). Updating and analysis of strong-motion database of Northern Italy through the residual analysis between empirical predictions and observations in the Po plain region. SIGMA ENEL Project, Deliverable SIGM0002-2013

	<p style="text-align: center;">Research and Development Programme on Seismic Ground Motion</p> <p style="text-align: center;">CONFIDENTIAL <i>Restricted to SIGMA scientific partners and members of the consortium, please do not pass around</i></p>	<p>Ref : SIGMA-2013-D2-72 Version : 01</p> <p>Date : 15 may Page : 44</p>
--	--	---

Pacor, F., R. Paolucci, G. Ameri, M. Massa, and R. Puglia (2011). Italian strong motion records in ITACA: overview and record processing, *Bulletin of Earthquake Engineering*, Vol. 9, 1741-1759.

Pondrelli S., A. Morelli, and G. Ekström, European-Mediterranean Regional Centroid Moment Tensor catalog: solutions for years 2001 and 2002, *Phys. Earth Planet. Int.*, 145, 1-4, 127-147, 2004.

Pondrelli S., Salimbeni S., A. Morelli, G. Ekström and Boschi E., European-Mediterranean Regional Centroid Moment Tensor catalog: Solutions for years 2003 and 2004, *Phys. Earth Planet. Int.*, 164, 1-2, 90-112, 2007.

Pondrelli S., Salimbeni S., Morelli A., Ekström G., Postpischl L., Vannucci G. and Boschi E., European-Mediterranean Regional Centroid Moment Tensor Catalog: solutions for 2005-2008, *Phys. Earth Planet. Int.*, in press, 2011.

Pondrelli, S., A. Morelli, G. Ekström, S. Mazza, E. Boschi, and A. M. Dziewonski, 2002, European-Mediterranean regional centroid-moment tensors: 1997-2000, *Phys. Earth Planet. Int.*, 130, 71-101, 2002.

Pondrelli, S., S. Salimbeni, G. Ekström, A. Morelli, P. Gasperini and G. Vannucci, The Italian CMT dataset from 1977 to the present, *Phys. Earth Planet. Int.*, doi:10.1016/j.pepi.2006.07.008, 159/3-4, pp. 286-303, 2006.

Sato, T., R. W. Graves, and P. G. Somerville (1999). Three-dimensional finite-difference simulations of long-period strong motions in the Tokyo metropolitan area during the 1990 Odawara earthquake (MJ 5.1) and the Great 1923 Kanto earthquake (MS 8.2) in Japan, *Bulletin of the Seismological Society of America*, 89, 579-607.

Rodriguez-Marek, A., G. A. Montalva, F. Cotton, and F. Bonilla (2011), Analysis of Single-Station Standard Deviation Using the KiK-net Data, *Bull. Seismol. Soc. Am.*, 101(3), 1242-1258, doi:10.1785/0120100252

Scasserra G., Stewart J. P., Bazzurro P., Lanzo G., and F. Mollaioli (2009). A Comparison of NGA Ground-Motion Prediction Equations to Italian Data, *Bull. Seismol. Soc. Am.*, 99, 5, 2961-2978, doi: 10.1785/0120080133

Somerville, P. G., N. F. Collins, R. W. Graves, and A. Pitarka (2004). An engineering ground motion model for basin generated surface waves, *Proc. 13th World Conference on Earthquake Engineering*, Vancouver, Canada, Paper 515.

REVIEW D2 72 CS N° 5 A. GURPINAR

CALIBRATION OF GMPE's FOR THE PO PLAIN REGION – SIGMA-2013-D2-72 (by Pacor, Luzi, D'Amico and Puglia)

General Remarks

- The Report is generally well written. It constitutes the continuation of the work by Pacor et al (2012) deliverable SIGMA-2012 D2-53 02. Basically the dataset which was considered in 2012 (called DBN) has been extended by the data from the aftershocks of the Emilia 2012 earthquake.
- The Report “Pacor et al (2012) deliverable SIGMA-2012 D2-53 02” was reviewed by two Scientific Committee members of SIGMA, Messrs. Scherbaum and Savy. The present Report which is under review does not make any reference to the Review Papers of the two scientific committee members. And therefore there is no indication that these comments have been taken into consideration in the continuation of the work.
- In particular, and as an example, two issues which have been specifically addressed by the two Scientific Committee members were as follows:
 - A credible justification for the selected five GMPEs.
 - Conversion to moment magnitude.The new Report does not address these issues.
- The site effects have been taken into consideration using Vs30 and the classification recommended by EC8. The Introduction of the report indicates that the Po Plain (where the records were taken) “...is one of the largest sedimentary basins in the world with an area of about 50000 km² and a sediment thickness varying from a few tens of meters to about 8 kms”. With this information one would expect to see a term related to sediment thickness in the functional form of the GMPE, which is not the case. Some explanation of how this has been addressed needs to be provided.
- The last review that was made by this reviewer involved a Report that concentrated on damage indices such as CAV and JMA intensity, from a structural engineering perspective. It is important to integrate this concept into GMPEs. Within the framework of the IAEA Extrabudgetary Program, both Campbell and Fukushima generated GMPEs using these damage indicators obtaining encouraging results, e.g. a reduction in the σ values. In the case of the Po plain, this would also address the issue raised by the authors in the Introduction, i.e. the possibility of trapped surface waves and prolonged ground shaking.
- It would have been useful to provide some further explanation to the results. For example, Figure 7a shows six points at a distance (Joyner-Boore distance) of 100 meters. Some clarification of the particular event(s) (to which these data belong)

and the way in which the distances were calculated would help in understanding the ground motion at very short distances.

- It would have been interesting to see some differences between the DBN and the new dataset as the latter differs significantly both for the site effects as well as the style of faulting.

Reviewer:

Aybars Gürpınar
3 June 2013

REVIEW ON BEHALF OF SIGMA PROJECT

Reference: SIGMA-2013-D2-72

Title: Calibration of GMPEs for Po Plain Region

Author: F. Pacor, L. Luzi, R. Puglia, M. D'Amico

Reviewer: Philippe Renault

Review date: 4.6.2013 (updated on 7.6.2013)

Review Comments:

General comments: The report has a clear structure and the reader can generally follow the argumentations of the author. The conclusions are interesting and meaningful for the SIGMA project. It should be acknowledged that a large amount of work has been done to collect and process all the new data, which leads to a significant improvement of the existing database.

The report is apparently a continuation of an earlier SIGMA deliverable (Pacor et al (2012), SIGMA-2012 D2-53 02). This is mentioned in the introduction, but it would be worth to include in the conclusions a discussion what is the improvement with respect to the GMPEs in the new assessment (earlier 5 GMPEs were used, now new GMPEs have been derived. Does the new work replace the previously selected GMPEs or do they represent an extension?). For the moment the previous and recent work seem to be disconnected.

As the final recommendation is that the use of the new GMPEs should be restricted to the Po Plain, it is not clear how the project will make use of the new results under these conditions. The limitation in the available site classes and style of faulting should be stressed and be put into context. This could be discussed in more detail in the conclusions of the report.

The final version of the report should be checked again for minor typos and especially missing spacing between words (or numbers, parentheses).

In the following the comments are grouped by chapter in order to put them in the appropriate context.

- Executive Summary:

The presence of an executive summary is very much appreciated. Nevertheless, it is worth to comment that a brief description of the requested task and specific output in the context of the SIGMA project could be included in the summary, in order to understand why the study was performed and how the results will be used. This might of course also be taken over from the work package leader and not necessarily from the author of the study.

Editorial remark: Line 20 “The total standard deviation (σ) varies between 0.32 and 0.41 log₁₀ unit,” seems to be a duplicate and should be deleted for the final version.

- DBN2 Dataset:

In the caption of figure 2 (page 8) it is not clear if there were any records with EC8-D and EC8-E site classes. The caption suggests this, but the corresponding symbols are not seen in the figure itself. If such are not present, this caption item should be deleted, as those site conditions raise doubts about usefulness of such conditions. But according to page 12 the database has very few of those sites and alternatively, the dots in the figure could be reduced in size to have a better overview of the M-R distribution.

- Ground Motion Prediction Equations

The assessment used the relationship of Castello et al. (2007) for the conversion of local magnitude to moment magnitudes. As the magnitude conversion is a tricky thing and can have a large effect on the outcome of the assessment it would be worth to justify why only this relationship was taken and preferred over other available relationships. Furthermore, the underlying uncertainties in the conversion should be carried along in order to allow for a quantification of these uncertainties or potentially reduction in the future. The reasoning behind the decisions can help to strengthen the conclusions and their applicability to the study region.

The Po Plain is a very special site situation which differs clearly from generic site conditions, for which GMPEs are usually set up. New GMPE coefficients were derived with the extended dataset and also show significant differences at high frequency between the different site classes (B, C, C1). The question needs to be asked if those broad site classes capture all effects that have been observed or if some remain buried (e.g. κ and 2D/3D effects). The authors have introduced the class C1 to accommodate some observed features, but it would be worth to discuss if this was sufficient or if a refined assessment would bring more insights (e.g. sub-classes or even a continuous Vs30 dependence as parameter, or a term which accounts for the shear wave velocity at deeper depth – like in some NGA models). Furthermore, the thickness of the sedimentary layer is unusual thick which might bias the assessment. An additional sensitivity evaluation with respect to the layer thickness at the station locations would be recommendable to assess this effect.

- Results

The plots of the comparisons between median predictions and the observations denote the Joyner-Boore distance as measure on the x-axis. As mentioned in the dataset section, both epicentral and Joyner-Boore distance have been used. It should be clarified if the distances were now converted for those plots or if the x-axis label should be simply distance implying both measures as in the previous chapters.

It seems like the fit for M5 and M6 +/-0.1 are in rather good agreement, for both site classes in the higher frequency range. Is this general observation confirmed also at other magnitudes e.g. 5.5 and 6.5? The +/-0.1 magnitude unit seems rather strict with respect to the available data. Is there an explanation why this range was not taken a bit broader?

Editorial remark: It would also be nice to have the background log-log grid in all figures, as they are missing in figures 8a, 8b and 10a, 10b. Those gridlines are helpful when trying to compare numbers from plot to plot.

- Analysis of residuals, Decomposition of the residuals

In figure 14 there are red lines for the magnitude scaling indicating a trend, but the origin of the red line is not explained in the legend. Furthermore, by eye the line for $T=0.1s$ doesn't seem to be corresponding to the average of the grey dots, which seems to have more like a positive residual.

General comment with respect to interface with other WP:

After the presentation at the scientific committee meeting on 6. June 2013 it became clear that the authors should try to support the project in terms of giving advice on how the GMPEs and the new data can be used and what are the boundary conditions. As there is maybe an undersampling issue of the new data with respect to site characterization and rupture mechanism the new GMPEs might have a bias. Furthermore, the interface to WP3 and WP4 should be stressed, as the GMPEs are developed for "Rock", but based on stations at the surface, which implicitly include a site amplification effect, and the end users might have a different understanding of the underlying "Rock". This should be discussed in the framework of the SIGMA approach 1 and 2 (using GMPEs directly up to the surface vs. using the GMPE to define the rock ground motion and then add the site specific amplifications to come up with a response at the surface). This can of course be resolved through bilateral communication between the authors and the WP4 members, but for the sake of transparency and documentation it would be beneficial to try to include it in the report.